

Surfactant-Templating of Zeolites: From Design to Application

Alexander Sachse, and Javier Garcia-Martinez

Chem. Mater., **Just Accepted Manuscript** • DOI: 10.1021/acs.chemmater.7b00599 • Publication Date (Web): 04 Apr 2017

Downloaded from <http://pubs.acs.org> on April 6, 2017

Just Accepted

“Just Accepted” manuscripts have been peer-reviewed and accepted for publication. They are posted online prior to technical editing, formatting for publication and author proofing. The American Chemical Society provides “Just Accepted” as a free service to the research community to expedite the dissemination of scientific material as soon as possible after acceptance. “Just Accepted” manuscripts appear in full in PDF format accompanied by an HTML abstract. “Just Accepted” manuscripts have been fully peer reviewed, but should not be considered the official version of record. They are accessible to all readers and citable by the Digital Object Identifier (DOI®). “Just Accepted” is an optional service offered to authors. Therefore, the “Just Accepted” Web site may not include all articles that will be published in the journal. After a manuscript is technically edited and formatted, it will be removed from the “Just Accepted” Web site and published as an ASAP article. Note that technical editing may introduce minor changes to the manuscript text and/or graphics which could affect content, and all legal disclaimers and ethical guidelines that apply to the journal pertain. ACS cannot be held responsible for errors or consequences arising from the use of information contained in these “Just Accepted” manuscripts.

Surfactant-Templating of Zeolites: From Design to Application

Alexander Sachse¹ and Javier Garcia-Martinez^{1,2*}

¹Dr. Alexander Sachse, Molecular Nanotechnology Lab, Department of Inorganic Chemistry, University of Alicante, E-03080 Alicante, Spain.

²Dr. Javier Garcia-Martinez, Molecular Nanotechnology Lab, Department of Inorganic Chemistry, University of Alicante, E-03080 Alicante, Spain.

Rive Technology, Inc., 1 Deer Park Drive, Monmouth Junction, NJ 08852, USA.

*E-mail: j.garcia@ua.es

Abstract

Surfactant-templating is one of the most effective and versatile synthetic strategies for the construction of well-defined porous architectures in solids. Though the principles of molecular self-assembly were disclosed in biological systems since long, the use of amphiphiles to generate porous architectures in inorganic matter has merely emerged at the very end of the 20th century. The present review proposes a *voyage* from the early developments of surfactant-templating for designing ordered mesoporous solids to the application of its principles for the generation of hierarchical zeolites. A thorough overview on the various strategies employing supramolecular chemistry to designing mesoporosity in zeolites is presented. The efficiency of the post-synthetic surfactant-templating approach in bridging the gap between zeolites and amorphous mesoporous molecular sieves is depicted through assessing their key properties, such as hydrothermal stability, texture, and acidity. Finally, the impact of hierarchical zeolites in the industry will be highlighted through a review of the catalytic performance of mesostructured zeolites as components of FCC catalysts in various refineries.

1. Surfactant-templating: A unique toolbox for the design of mesoporous materials

Surfactant-templating (also referred as supramolecular templating) emerged as general term to describe the *chimie douce* approaches for conceiving solids with tunable porosity. These soft chemistry strategies in materials design comprise the evolution of porous features, determined by supramolecular assemblies that act as templates, which develop from individual amphiphilic molecules, *i.e.* surfactants. Surfactant-templating might indeed be defined as: a synthetic strategy leading to materials featuring tailored porosity, both in terms of pore size and architecture, by employing the self-assembly properties of surfactant molecules, which act as porogen, and their interactions with moieties of the forming material. At present, surfactant-templating has established as a versatile strategy especially suited for the preparation of well-defined porous materials of various chemical natures typically in the mesopores range organized in a variety of architectures.

Though the principle of surfactant-templating was firstly applied in 1969 for the achievement of mesostructured amorphous silica using trimethylalkylammonium-based amphiphilic molecules, it was not until more than 20 years later that the potential of this strategy was realized, possibly due to the lack of appropriate characterization of the developed material.^[1,2] In 1990 Yanagisawa *et al.*^[3] reported the achievement of surfactant-templated silica by exposing kanemite to trimethylalkylammonium-based surfactants at basic pH. The authors observed the development of several peaks in the low angle XRD region, ascribable to the formation of an ordered mesoporous network in the silica material. Further, they observed the size-dependency of the developed porosity as a function of the length of the hydrocarbon chain of the surfactant, which is a characteristic feature of surfactant-templating. Yet, it was only through the famous publication by Mobil Oil scientists in 1992 that surfactant-templating embarked in its amazing success story for the design of tailored porous materials.^[4,5] Therein the authors described the achievement of three mesoporous silica materials featuring porous architectures of different space groups, today known as M41S family. This class of ordered mesoporous materials undoubtedly epitomizes the versatility of the surfactant-templating approach for the development of mesoporous architectures with extremely narrow and tunable pore size.^[6]

These early developments gave rise to the evolvment of a new field in materials chemistry and served as inspiration for the design of a plethora of mesoporous

1
2
3 materials of well-defined architectures. Promptly the principles of surfactant-
4 templating were applied for the design of a great variety of metal oxides based on
5 magnesium, aluminum, manganese, iron, cobalt, nickel, zinc, tungsten, as well as
6 of non-oxide compounds, such as phosphates, sulfides, nitrides, carbides and
7 selenides by judiciously selecting the appropriate surfactants and adjusting the
8 synthesis conditions.^[7-11] These advancements went hand in hand with the
9 development of a diversity of synthetic strategies based on the use of charged
10 (cationic or anionic salts) and non-ionic surfactants in a wide range of pH
11 conditions. A detailed description of the choice of surfactants and synthesis
12 conditions for the achievement of different mesophases has been outlined in the
13 excellent review by Wan and Zhao.^[9]

14
15
16
17
18
19
20
21 A variety of assembly mechanisms have been disclosed attending to the nature of
22 the employed surfactant and to the synthetic conditions (particularly the pH). A
23 charge matching model was developed by Huo *et al.*,^[10] who introduced a
24 specific nomenclature to describe the synthetic path leading to the mesostructured
25 material. When employing ionic surfactants, the development of the mesophase is
26 essentially governed by columbic interactions, which is the case when either the
27 surfactant (S) or the inorganic species (I) are oppositely charged. The two
28 possibilities hereto are the S^+I^- or S^-I^+ paths. When synthetic conditions are
29 chosen in such a way that both inorganic moieties and the surfactant molecules
30 present the same charge, anions (X) or cations (M) present in the solution
31 participate in the structuration process. The resulting mechanisms can be
32 described as to follow S^+XI^+ or $S^-M^+I^-$ paths. In the case non-ionic surfactants
33 are employed, the path can be described as S^0I^0 and is based on hydrogen bond or
34 dipolar interactions. The latter is often denominated N^0I^0 when amines (N) are
35 used as surfactants. Soler-Illia *et al.* were the first to propose to schematically
36 represent these pathways as a function of the chemical interactions (**Figure**
37 **1A**).^[11]

38
39
40
41
42
43
44
45
46
47
48
49
50
51
52
53
54
55
56
57
58
59
60
It is the hydrophilic – hydrophobic interactions between the surfactant and the
solvent (in most cases water) that are the driving force for the assembly into
various micellar shapes of thermodynamically stable phases giving rise to
mesostructures of different architectures with long range order. The micellar
packing parameter is particularly useful to predict the achieved mesophase in the
case ionic surfactants are employed (**Figure 1B**).^[12] Important evidence has been

1
2
3 produced that in the mesostructuration employing non-ionic surfactants the
4 mesophase is determined by the hydrophilic/hydrophobic volume ration (V_H/V_L)
5 of the surfactant.^[13,14]
6
7

8 The principles of surfactant-templating could further be applied to the synthesis
9 of periodic mesoporous carbons. In this case, most approaches rely on the $S^{0}I^0$
10 path by employing non-ionic surfactants. Indeed, it is the hydrogen bridges that
11 form between the phenolic resins (used as carbon source) and the block
12 copolymers that lead to mesostructuration. Here surfactants are removed by
13 extraction and final carbonization of the mesoporous polymer leads to the
14 mesoporous carbon material. This strategy was recently reviewed by Ma et al.^[15]
15
16
17
18

19 In 2008, surfactant-templating was further adapted to produce a new class of
20 hierarchical organic-inorganic hybrid materials described as mesostructured
21 metal organic frameworks (meso-MOFs).^[16] Lately, Bradshaw et al.^[17] reviewed
22 the different strategies based on supramolecular assembly of amphiphiles for the
23 achievement of the mesoporous hybrid materials.
24
25
26
27

28 Thanks to the knowledge gained in the design of a wide variety of porous
29 amorphous solids (**Fig 1C**), a handful of strategies based on surfactant-templating
30 have emerged to produce hierarchical crystalline materials and in particular for
31 conceiving mesoporosity in zeolites. These approaches are particularly stimulated
32 by the long-standing goal to finally bridge the gap between mesoporous materials
33 and zeolites. The application of surfactant-templating for the development of
34 hierarchical zeolites has emerged as a set of extremely promising techniques that
35 up to date constitute the sole possibility to truly tailor mesoporosity in zeolites.
36 These strategies will be highlighted in the following sections.
37
38
39
40
41
42
43
44

45 **2. The need for surfactant-oriented strategies for the conception of hierarchical** 46 **zeolites**

47 The development of ordered mesoporous inorganic materials, and in particular
48 aluminosilicates, created very high expectations in the early 1990s as many
49 researchers believed that this new class of porous materials would revolutionize
50 chemical industry, and especially replace the use of zeolites in processing bulky
51 hydrocarbons. Yet, it soon became clear that the achieved materials present major
52 drawbacks, especially related with their weak acidity and poor hydrothermal
53 stability.^[18]
54
55
56
57
58
59
60

1
2
3 It was soon pointed out that the ideal material should contain the advantages of
4 both zeolites (strong acidity and excellent hydrothermal stability) and
5 mesoporous molecular sieves (high accessibility of reactant molecules to active
6 sites and fast diffusion of product molecules out of the catalyst), through the
7 development of mesoporous materials with zeolitic pore walls.^[19] This powerful
8 image has been the driving force for the development of hierarchical zeolites for
9 over two decades.

10
11 With the aim to realize the depicted materials class, researchers initially
12 developed an approach that relied on the direct crystallization of amorphous
13 mesoporous materials (*e.g.* MCM-41).^[20] This strategy proved highly
14 unsuccessful and up to date, there is no report claiming the complete
15 crystallization of the mesoporous skeleton of periodic porous amorphous
16 materials.^[21,22] It has later been indicated that the zeolite lattice is incompatible
17 with the mesoporous curvature and it is thus that these approaches lead to partial
18 or total loss of the textural mesoporous properties of the original silica. Yet, this
19 limitation was overcome through the crystallization of SBA-15/CMK-5
20 composites by the treatment with tetrapropylammonium hydroxide (TPAOH).
21 Here, the carbon mold acts as scaffold allowing for maintaining the mesoporosity
22 even after complete zeolitization of the amorphous silica.^[23]

23
24 Various strategies, which do not require the use of surfactants have been put
25 forward with the aim of achieving hierarchical zeolites.^[24-30] A very first strategy
26 aiming at conceiving mesoporosity in zeolites was based on creating cavities
27 through the dissolution of alumina or silica species from the zeolite framework.
28 Indeed the formation of secondary porosity in zeolites can readily be achieved
29 through simple treatment of the solids with bases, acids or steam. Though rather
30 simple and cost efficient, these strategies produce uncontrolled porosity that often
31 is not connected in the zeolite crystals. The forming secondary porosity can
32 hardly be tuned and defined porous architectures cannot be achieved by these
33 means. These techniques feature the additional inconvenience that the nature and
34 strength of the acid sites are altered during the treatment and the integrity of the
35 zeolite is damaged.

36
37 Additionally, the hard-templating approach was developed for the conception of
38 mesoporous zeolites and firstly reported through the use of carbon nanoparticles
39 within the synthesis gel.^[31] An important variety of hard templates have been
40
41
42
43
44
45
46
47
48
49
50
51
52
53
54
55
56
57
58
59
60

1
2
3 investigated for this approach, such as carbon nanotubes or nanofibers,
4 mesoporous carbons and carbon aerogels. This approach yet presents important
5 drawbacks, chiefly the high cost of sacrificial templates.^[32]
6
7

8 In contrast to the aforementioned approaches, surfactant-oriented strategies
9 present a much higher degree of flexibility and permit to achieve tailored textural
10 properties and a variety of architectures based on the nature of the amphiphiles
11 and their interaction with the zeolitic species. In the following sections, we will
12 consider the variety of surfactant-oriented approaches that have been disclosed in
13 the recent scientific literature with specific focus on the nature of the interactions
14 between surfactant and the inorganic species.
15
16
17
18
19

20 21 **3. Surfactant-oriented strategies for achieving mesoporous zeolites**

22 **3.1 Double or dual templating**

23 Moved by the explosive development of surfactant-templating for the conception
24 of mesoporous inorganic materials, researchers attempted to directly transpose
25 this synthetic strategy to the design of mesoporous zeolites. The surfactant is
26 added right from the beginning to the zeolite synthesis gel composition that,
27 depending on the target zeolite phase, is usually composed of a silica and alumina
28 source in basic pH with the eventual employment of zeolites structure directing
29 agents (SDA). This process is hence frequently referred as dual or double
30 templating as the surfactants and the zeolite SDA are simultaneously present in
31 the zeolite synthesis solution.
32
33
34
35
36
37
38

39 Very few of these attempts have revealed fruitful, as in most cases, phase
40 segregation is the leading process; yielding a purely microporous and mesoporous
41 phase. Kloetstrat *et al.*^[33] were the first to observe the formation of two distinct
42 phases by adding cetyltrimethylammonium chloride (CTAC, $(\text{CH}_3)_3\text{NC}_{16}\text{H}_{33}\text{Cl}$)
43 directly to the synthesis gel of zeolite Y. The authors reported the achievement of
44 1 micron sized zeolite Y crystals, overgrown with a thin layer of amorphous
45 MCM-41. Later, Karlsson *et al.*^[34] described the double templating approach for
46 MFI materials employing trimethylalkylammonium-based surfactants. Aware that
47 the MFI phase requires high crystallization temperatures whilst mesoporous
48 phases can readily be obtained at room temperature, they implemented multi-step
49 treatments at various temperatures and using different surfactant to SDA ratios.
50
51
52
53
54
55
56
57
58
59
60

1
2
3 The authors concluded that both templates act in competitive manner, invariably
4 yielding two distinct phases.

5
6 Numerous reasons have been put forward aiming at explaining the unsuitability
7 of such approaches in attaining truly hierarchical zeolites. From a synthetic point
8 of view, zeolite crystallization and mesophase formation feature very different
9 mechanisms and kinetics. Whilst periodic mesostructures of amorphous solids
10 usually form fast and at low temperatures, zeolite synthesis requires longer
11 crystallization times and often hydrothermal conditions.

12
13 Interestingly, Du *et al.*^[35] reported very recently the achievement of the
14 hierarchical titanosilicate TS-1 featuring intracrystalline mesoporosity through
15 the employment of the non-ionic surfactant Triton X-100 (polyethylene glycol
16 *tert*-octylphenyl ether) simultaneously to the zeolite SDA tetrapropylammonium
17 hydroxide (TPAOH). The obtained TS-1 crystals were smaller in size than the
18 reference microporous TS-1 achieved in the absence of the surfactant and
19 featured wide size distribution of mesopores with mesoporous volumes of up to
20 0.17 cm³ g⁻¹. Yet, the development of a wide size distribution of mesopores is a
21 strong indication that the surfactant-templating was not very effective.
22
23
24
25
26
27
28
29
30
31

32 33 **3.1.1 The effect of polymers and polymer/surfactants in the dual synthesis** 34 **approach**

35
36 Direct synthesis approaches based on the use of employing charged high
37 molecular weight polymers have further been described. Such polymers cannot
38 strictly be defined as surfactants due to their inability to form supramolecular
39 assemblies through self-assembly.^[36] Yet, the formation of the mesophase relies on
40 a soft-templating approach and on the efficient interactions of the positive surface
41 charge of the polymers with the forming zeolite species in the synthesis gel.
42

43
44 The first to explore this synthesis route were Xiao *et al.*^[36,37] who added
45 polydiallyldimethylammonium chloride (PDADMAC) to the synthesis gel of
46 zeolite *BEA. The authors reported the synthesis of a zeolite featuring disordered
47 intracrystalline mesoporosity presenting a wide size distribution. The
48 intracrystalline nature of the mesoporosity was assessed through electron
49 diffraction tomography (EDT) that allows for the three-dimensional (3-D)
50 reciprocal space reconstruction of the crystals. This reconstruction rendered a part
51 of the reciprocal lattice of the framework of the zeolite *BEA and represents by
52
53
54
55
56
57
58
59
60

1
2
3 projections along a^* , b^* and c^* axes of the crystal. The authors furthermore
4 highlighted the fact that the reflections along the b^* plane were elongated which
5 would suggest a certain degree of structural disorder of the crystal lattice which
6 can readily be attributed to the presence of highly dense mesopores (**Figure 2**).
7
8 Additionally, high angle annular dark field scanning transmission electron
9 microscopy (HAADF-STEM) further allowed for imaging the crystalline
10 nanostructure containing three-dimensionally interconnected mesoporosity of
11 high density in the entire crystal.
12

13
14
15
16 The same group reported the achievement of mesoporous ZSM-5 by the use of
17 polystyrene-co-4-polyvinylpyridine (C-PSt-co-P4VP) previously treated with
18 methyl iodide directly in the synthesis mixture.^[38] ZSM-5 crystals featuring
19 intracrystalline mesoporosity aligned along the b -axis of the zeolite crystallinity
20 were achieved. Yet, mesoporosity is not well-defined and its size distribution
21 covers the entire mesoporous range.
22

23
24
25
26 Liu *et al.*^[39] succeeded in synthesizing mesoporous MFI zeolites of various Si/Al
27 ratios by the use of the anionic polymer poly(acrylic acid) in combination with
28 the cationic surfactant CTAB and the zeolite SDA TPAOH. The authors reported
29 that the use of the negatively charged polymer does not allow for the formation of
30 hierarchical zeolite with MFI structure. Yet, by the addition of the cationic
31 surfactant, a polymer-surfactant complex develops where the negative charge
32 density of the polymer is efficiently reduced allowing the electrostatic attraction
33 of the organic template with the negatively charged inorganic species. Hence,
34 MFI type zeolites with mesopores in the range of 5-20 nm were achieved.
35

36
37
38
39
40
41 The group of Pinnavaia^[40] developed polymers with the ability to covalently bind
42 to the forming inorganic zeolite network. The group designed silylated
43 polyethylamines able to connect to the inorganic species through hydrolysis and
44 condensation. This strategy yielded mesoporous ZSM-5 (named MSU-MFI),
45 which presents a well-defined capillary condensation regime in the nitrogen
46 physisorption isotherm. The textural properties of the achieved MSU-MFI could
47 be further modulated by altering the molecular weight of the polymer.
48
49
50
51
52
53
54
55
56
57
58
59
60

3.1.2 Combining zeolite seeds and surfactants: amorphous mesoporous materials with zeolite characteristics

An alternative to the direct synthesis approach is the use of nanosized zeolites so-called “zeolite seeds” as precursors of the crystalline phase through their combination with surfactants during the hydrothermal treatments (**Figure 3A**). Such nanosized zeolites are usually synthesized through classical zeolite synthesis conditions but at shorter synthesis times and often lower temperatures. These seeds show no X-ray diffraction peaks; yet typical vibrational bands ascribable to the zeolite phase are observable by IR and Raman spectroscopy, which indicates the existence of small zeolite units but the absence of long-range crystallinity (**Figure 3B**).^[41]

Inspired by the insights disclosed for the synthesis of the M41S family, the group of Pinnavaia was the first to investigate the use of protozeolitic species in combination with the cationic ammonium-based surfactant, namely CTAB.^[42] They prepared zeolite Y seeds with a Si/Al ratio of 9, lowered the pH of the seed solution to 9 and then added an aqueous surfactant solution prior to aging the mixture at 100 °C for 20 h. Through this approach, a material composed of a single phase (Al-MSU-S) presented hexagonally ordered mesopores, yet they lacked zeolite crystallinity as determined by X-ray diffraction (**Figure 3C**). Nonetheless, from their careful characterization through ²⁷Al MAS NMR, the retention of a zeolite-like connectivity of the AlO₄ tetrahedra upon the assembly of the mesostructure could be deduced, which was taken as evidence of the presence of a FAU local structure within the mesopore walls. The authors evidenced moreover the superior hydrothermal stability and improved cumene cracking activity of the Al-MSU-S materials compared to Al-MCM-41 with equal Si/Al ratio, which was taken as further proof of the presence of zeolite fragments within the pore walls of the mesoporous structure.

The same research group expanded this approach by using MFI and BEA zeolite seeds to obtain MSU-S materials with hexagonal periodic order of the mesopores.^[43] Here, they evidenced the presence of the pentasil subunit in the pore walls of the mesopores by IR spectroscopy. During the same year, Zhang *et al.*^[44,45] employed *BEA and ZSM-5 seeds in combination with CTAB and named the achieved material, obtained through hydrothermal treatment, MAS-5. The authors confirmed the presence of zeolite fragments in the pore walls of MAS-5 through Raman spectroscopy. Li *et al.*^[46,47] disclosed that optimized

1
2
3 aging times of the zeolite Y seeding gel leads to materials with higher
4 hydrothermal stability, acidity, and long range hexagonally structured
5 mesoporosity.
6

7
8 The group of Pinnavaia further disclosed synthetic conditions that lead to the
9 development of the cubic *Ia3d* mesophase by adding ethanol as co-solvent to the
10 synthetic mixture that containing the surfactant CTAB and the FAU zeolite seeds
11 formed from metakaolin.^[48] The use of the alcohol was previously disclosed for
12 the synthesis of MCM-48 as it permits to efficiently augment the micelle packing
13 parameter, which causes the denser micelle arrangement.^[49] The by this means
14 achieved cubic mesoporous aluminosilicates featured zeolite fragments in their
15 pore walls and was named Al-MSU-S₄₈.
16

17
18 Approaches based on different paths other than S⁺T⁻ where investigated
19 employing protozeolitic species. The group of Pinnavaia extended this approach
20 by combining zeolite seeds in acidic conditions with non-ionic surfactants.^[50]
21 Hereto, the pH of the zeolite seeding solution was lowered below 7 before adding
22 the neutral surfactant Pluronic 123 ((EO)₂₀(PO)₇₀(EO)₂₀) and trimethylbenzene
23 (TMB) as micelle swelling agent and hydrothermally treating the mixture. The
24 authors evidenced that the porous features of the obtained materials could be
25 influenced by the pH of the synthesis solution. Indeed, when the pH was between
26 2.5 and 6, a foam-like structure built up by strut-like walls, which frame windows
27 opened into spherical cells with narrow pore size distributions. The material was
28 denominated MSU-S/F. When the pH of the synthesis solution was higher (pH =
29 6 – 7), MSU-S/H materials where obtained. These materials featured long range
30 ordered hexagonal mesoporosity. Analogous to the previously described MSU-S
31 materials, the MSU-S/F and MSU-S/H present zeolite fragments in their pore
32 walls, as evidenced by IR spectroscopy.
33

34
35 The achievement of distinct mesophases as a function of the pH strongly suggests
36 that the synthesis follows different mechanistic routs. Both syntheses were
37 performed at pH above the isoelectric point of the zeolite precursor species,
38 which indicates that in either case the inorganic species were negatively charged.
39 Moreover, wormhole mesostructured aluminosilicates (Al-MSU-S_w) were
40 achieved by employing the non-ionic compound tallow tetraamine in slightly
41 basic conditions in combination with Y zeolite seeds.^[48] In this case, the
42 supramolecular assemblies formed through π - π stacking. It is yet not evident to
43
44
45
46
47
48
49
50
51
52
53
54
55
56
57
58
59
60

1
2
3 ascribe to which favorable interactions between the neutral amine and the
4 negatively charged zeolite seeds the formation of the mesostructured material
5 under the applied pH conditions may result. Indeed, in a more recent publication
6 by the same group, the experimental section states acidic synthesis conditions for
7 the formation of the Al-MSU-S_w material employing tallow tetraamine.^[51] In such
8 conditions, the formation mechanism can readily be described to follow a N⁰H⁺T
9 interaction.
10

11 It is important to mention now, that the examples presented up to this point do not
12 achieve truly hierarchical zeolites as they lack crystallinity and therefore cannot
13 be described as zeolites. However, they have paved the way to fully crystalline
14 hierarchical zeolites and are excellent examples of the versatility of surfactant-
15 templating for the achievement of various complex mesoporous architectures. In
16 fact, the employment of zeolite seeds in combination with surfactants has further
17 been reported to achieve truly hierarchical zeolites. Here, the critical key factors
18 enabling the obtaining of crystalline mesopore walls are based on the nature of
19 the zeolite seed (*i.e.* the condensation degree) and the nature of the surfactant
20 head group (and the eventual use of co-solvents).
21
22
23
24
25
26
27
28
29
30
31

32 33 **3.1.3 Hierarchical zeolites through judicious choice of surfactant-templating** 34 **conditions employing seeds** 35

36 Mesoporous zeolite assemblies were achieved by the self-assembly of zeolite
37 FAU seeds with the cationic surfactant CTAB in the presence of co-solvents and
38 micelle swelling agents during hydrothermal synthesis.^[52] The authors indicated
39 that trimethylbenzene (TMB), used as swelling agent, and *tert*-butyl alcohol
40 (TBA), employed as co-solvent, both work synergistically to produce the
41 hierarchical zeolites. The authors argue the ability of the tertiary alcohol to
42 reduce repulsive forces of the surfactant headgroups, leading thus to an increase
43 in the micelle packing parameter and hence in the micelle charge density.
44 Through this strategy the affinity between the micelles and the aluminosilicates
45 species are enhanced. The authors further estimated that as TMB promotes the
46 zeolite surfactant assembly by swelling the surfactant micelle allowing to match
47 to the zeolite precursor species size.
48

49 Zhu *et al.*^[53] put forward that the achievement of hierarchical zeolites by using
50 seeds is critically influenced by the polymerization degree of the nanometer sized
51
52
53
54
55

1
2
3 species. The authors kinetically controlled the seed formation, which then in a
4 second step, were subjected to hydrothermal treatment in combination with
5 CTAB. Depending on the amount of surfactant and of co-solvent used in the
6 synthesis, hierarchical ZSM-5 featuring disordered mesoporosity with narrow
7 size distribution could be achieved (**Figure 4**).
8
9

10
11 A similar approach was developed through the combination of CTAB with
12 pluronic F127 and ZSM-5 zeolite seeds.^[54] Here, the zeolite building units firstly
13 aggregated with the CTAB micelles before assembling with the F127 (which
14 concentration gradually augments during the temperature treatment by the
15 evaporation of the solvent). The authors observed that the F123 micelles stacked
16 along the b direction of the crystals. Hence, a hierarchical ZSM-5 with a dual
17 pore size distribution composed out of smaller CTAB-templated disordered
18 mesopores and larger mesopores oriented along the b-axis of the ZSM-5 crystals
19 were achieved.
20
21

22
23 Further, the nature of the polar headgroup was indicated to have a major
24 influence in the efficient assembly of zeolite seeds. It was described that the
25 imidazolium-based ionic liquid [C₁₆MIm]Cl when employed as surfactant in the
26 hydrothermal treatment with MFI seeds, proved to be suitable for the
27 achievement of hierarchical ZSM-5 with partially ordered mesoporosity.^[55]
28 Indeed, it was previously indicated for the synthesis of MCM-41 that the
29 imidazolium headgroup allows for a stronger binding strength to charged silica
30 species and to a higher binding density.^[56] It is these features that critically
31 influence the surfactant-templating ability.
32
33

34
35 Protozeolitic FAU and *BEA seeds have further been combined with the cationic
36 polymer PDADMAC to achieve zeolites containing disordered mesopores.^[57,58] It
37 remains yet questionable whether the reported zeolites truly contains
38 mesoporosity, as the presented nitrogen physisorption experiments indicate type I
39 isotherms and the narrow pore size distribution put forward by the authors should
40 more correctly be ascribed to cavitation than to tailored mesoporosity.^[59]
41
42

43 44 45 46 47 48 49 50 51 52 53 **3.1.4 Hierarchical zeolites through the functionalization of seeds with 54 organic functions** 55

56 A devised approach was developed by the group of Serrano based on the
57 functionalization of zeolite seeds and their subsequent crystallization.^[60-62] They
58
59
60

1
2
3 developed protozeolitic units comprised between 2 and 5 nm. These were
4 subsequently silylated through standard grafting techniques employing
5 phenylaminopropyltrimethoxysilane in order to achieve zeolite seeds
6 functionalized with aromatic groups. Further, the functionalized seeds were
7 subjected to hydrothermal conditions to promote zeolite crystallization (**Figure**
8 **5**). Hence, zeolites composed out of aggregates of small size developed. The
9 authors assessed the role of the organic surface moieties to perturbate the zeolite
10 crystallization leading to the formation of interparticular mesoporosity within the
11 single aggregates. It was furthermore shown that the amount of formed
12 mesoporosity was determined by the amount of grafting agent used in the
13 synthesis. Diversely, the functionalization of zeolite seeds with hydrocarbon
14 chains of different length revealed not very successful to develop hierarchical
15 features and bulk zeolites were obtained. Based on the observation that solely the
16 functionalization with phenyl groups allowed for the achievement of the
17 intergrown zeolite structures, it could be put forward that π - π interactions
18 between the functional moieties during the crystallization process play a crucial
19 role in the assembly of the nanozeolites. Here, a so far unexplored approach can
20 be put forward, which would represent the simultaneous use of surfactants
21 comprising aromatic groups that could interact through π - π interactions with the
22 moieties on the surface of the functionalized seeds.

23
24
25
26
27
28
29
30
31
32
33
34
35
36 Recently, the assembly of protozeolites without the use of surfactants was
37 reported to yield Al-rich MFI featuring intercrystalline mesoporosity through the
38 rod-like assembly of the zeolite precursors.^[63]

39
40
41 Although the assembly of nanosized zeolites with surfactants produced
42 hierarchical zeolites, presenting zeolite X-ray diffraction peaks, it appears that
43 this strategy leads to the formation of zeolite aggregates (**Figure 5C**). Indeed,
44 such approaches have yet yielded individual zeolite crystals featuring
45 intracrystalline mesoporosity.
46
47
48
49
50

51 **3.2 Hierarchical zeolite synthesis with silane-terminated quaternary amines:** 52 **linking the surfactant to the zeolite precursor**

53
54 Ryoo and coworkers have greatly contributed to the development of surfactant-
55 templated hierarchical zeolites, through the design of a new family of surfactants
56 based on amphiphilic silanes comprising a hydrophobic tail and a modified
57
58
59
60

1
2
3 headgroup, which is covalently linked to a trialkoxysilane moiety. These
4 surfactants enable to circumvent the typical drawbacks encountered with classical
5 cationic amphiphiles in the synthesis of hierarchical zeolites, by presenting
6 unique features: i) the ability to form covalent bonds with inorganic species by
7 hydrolysis and condensation, ii) the capability of the ammonium head group to
8 act as zeolite SDA and iii) the ability of the hydrophobic chains to efficiently
9 form mesophases through self-assembly. These features together allow to achieve
10 hierarchical zeolites by preventing phase separation into two distinct phases.

11
12
13
14
15
16 The first silylated surfactant that was described was 3-(trimethoxysilyl)propyl-
17 hexadecyldimethylammonium chloride (TPHAC),^[64] that was directly added to
18 the synthesis mixture of ZSM-5 and LTA prior to hydrothermal treatment. The
19 achieved zeolite phases feature disordered, wormhole-like porosity with very
20 narrow mesopore size distributions (**Figure 6**). They proved the surfactant-
21 templating ability of this new type of surfactant through the tunability of the
22 mesoporous size distribution by varying the length of the hydrophobic chain
23 between 12 and 18 carbon atoms. They furthermore proved that synthesis time
24 and temperature crucially influences the size distribution of the mesoporosity.
25 Additionally, the amount of the organosilane added during the synthesis is a
26 critical parameter that influences the mesoporous size distribution and generated
27 mesoporous volume. The intracrystalline nature of the mesophase was assessed
28 by a combination of high resolution scanning electron microscopy (HR-SEM)
29 with cross-sectioning through an argon beam.^[65] Further, the presence of
30 disordered, interconnected wormhole-like mesoporosity was evidenced by
31 visualizing the porous architecture through the formation of Pt nanowires within
32 the zeolite crystals, which were subsequently imaged by TEM.^[66]

33
34
35
36
37
38
39
40
41
42
43
44 The same group successfully employed this approach for the development of
45 mesoporous sodalite, describing its first application as basic catalyst.^[67] TPHAC
46 revealed moreover as a suitable surfactant for the achievement of the hierarchical
47 zeotypes ALPO4-5 and ALPO4-11 featuring in both cases tailored
48 mesoporosity.^[68]

49
50
51
52
53
54
55
56
57
58
59
60 Inayat *et al.*^[69] were the first to employ the silylated surfactant TPHAC for the
synthesis of FAU type zeolites displaying a unique hierarchical porous structure
that is built up by zeolite nanosheets assembled in a house-of-cards like fashion,
featuring macroporous interstices located within the nanosheet stacks. The

1
2
3 distance between the individual nanosheets in this construction is of
4 approximately 7 nm through which the zeolite macropores are accessible. Very
5 recently, Qamar and co-workers reported the synthesis of nanocrystalline
6 mesoporous Y zeolite featuring octahedral facets using again TPHAC as
7 surfactant.^[70] The authors further evidenced that the amount of the employed
8 surfactant represents a critical factor that controls the dimensions of the obtained
9 nanocrystals.
10

11
12
13
14 TPHAC was furthermore used in combination with micelle expanding agents in
15 the zeolite LTA synthesis.^[66] Triblock co-polymer P123 (EO20PO70EO20) was
16 employed as swelling agent, which allowed to efficiently increase the mesopore size
17 from 7.4 to 23.7 nm. The authors assumed that the non-ionic surfactant permeates into
18 the hydrophobic region formed by the TPHAC surfactant chains, which thus leads to an
19 expansion of the micelles and hence to larger mesopores.
20

21
22
23
24 A novel surfactant based on amphiphilic silanes, developed by Han *et al.*^[71] and
25 featuring a double-acyloxy with double C₁₂ alkyl chains, 2,3-
26 bis(dodecanoyloxypropyl)-[3-(trimethoxysilyl)-propyl]dimethylammoniumiodide
27 (BTDAI) was used to produce hierarchical ZSM-5. More precisely, the presence
28 of BTDAI within the zeolite synthesis gel allowed for the achievement of
29 hierarchical ZSM-5 zeolites with platelet-like morphology and a wide mesopore
30 size distribution. Shortly thereafter, the authors studied the influence of varying
31 both the chain length of the BTDAI-type surfactants and its concentration in the
32 synthesis mixture. Under optimized conditions mesoporous volumes up to 0.19
33 cm³ g⁻¹ were achieved.^[72]
34
35
36
37
38
39
40
41
42

43 **3.3 Hierarchical zeolites by surfactants with multiple quaternary ammonium** 44 **centers**

45
46 A major breakthrough in the surfactant-templating of zeolites was achieved by
47 Ryoo and co-workers through the design of surfactants featuring various
48 quaternary ammonium centers. In their pioneering publication, the group
49 presented the achievement of MFI-type zeolites composed by nanosheets of a
50 size of a single unit cell.^[73] In this way, ultrathin zeolite layers were produced
51 that were three-dimensionally intergrown to form the hierarchical zeolite
52 structure. The employed surfactant, namely C₂₂₋₆₋₆ (C₂₂H₄₅-N(CH₃)₂-C₆H₁₂-
53 N(CH₃)₂-C₆H₁₃Br₂), is composed of two quaternary ammonium centers spaced by
54
55
56
57
58
59
60

1
2
3 C₆ alkyl chains, that together form the structure directing group of the MFI phase
4 whilst the long hydrocarbon tail (C₂₂) acts as mesostructuring template by
5 forming supramolecular micellar assemblies via hydrophobic interactions. The
6 secondary role of the hydrophobic chain is to restrict the growth of the zeolite,
7 leading to sheets of thicknesses of a few pentasil units of 2 nm spaced by 2.8 nm
8 thick micellar layers (**Figure 7 top**).

9
10
11
12 The same research group evidenced by low and wide angle XRD that the
13 nanosheet assembly develops from an initial hexagonal organized mesophase
14 with amorphous pore walls, which is subsequently transformed through heat
15 treatment into a lamellar mesophase with walls that are built up by the crystalline
16 zeolite framework (**Figure 7 bottom**).^[74,75]

17
18
19
20
21 Very recently Xi *et al.*^[76,77] carried out computational simulations in order to
22 describe the distribution of the LUMO (lowest unoccupied molecular orbital) on
23 multiple quaternary ammonium centered surfactants. Through this study the
24 authors were able to reason the role of the inner ammonium groups to direct the
25 synthesis of the MFI phase.

26
27
28
29
30 An excellent example that highlights the importance to rationally design
31 surfactants by taking into account their charge density and their structure was
32 presented by the group of Ryoo, who developed tricationic surfactants composed
33 out of two long alkyl chains of identical length and where the ammonium groups
34 were spaced by C₆ alkyl segments (18-N₃-18).^[78] This surfactant allowed for the
35 achievement of an ordered mesoporous structure which presents broad peaks in
36 the high angle XRD region of very low intensity, suggesting a regular stacking of
37 lattice planes with atomic-scale ordering at least to some extent (**Figure 8**).
38 Indeed, the determination of the crystalline framework structure is bounded and
39 can rather be ascribe as “pseudocrystallinity”. The flexibility of this approach was
40 further pointed out by using surfactants with four ammonium groups spaced by
41 C₆ alkyl segments (18-N₄-18) and additionally feature aromatic groups as
42 spacers; giving rise to the surfactants N₄-phe, N₆-diphe, and N₈-triphe. The
43 authors reported that through the increase of the amount of cationic centers in the
44 surfactants the obtained mesostructure lost structural order. In the same direction,
45 the wall thickness increased from 2.9 to 5.1 nm for the surfactants with four and
46 eight cationic centers, respectively.
47
48
49
50
51
52
53
54
55
56
57
58
59
60

1
2
3 Micron sized SSZ-13 zeolite (CHA structure) assembled to form mesoporous
4 aggregates was achieved by Wu *et al.*^[79] through the use the bi-quaternary
5 surfactant $C_{22}H_{45}-N(CH_3)_2-(CH_2)_4-N(CH_3)_2-C_4H_9Br_2$ together with the zeolite
6 SDA, N,N,N-trimethyl-1-adamantanammonium hydroxide (TMAOH).
7

8
9 The group of Ryoo further developed a new surfactant composed out of three
10 cationic centers bridged by C_6 unities and ended symmetrically by two C_{18} tails.
11 By the addition of this surfactant to the ZSM-5 synthesis gel, ultrathin MFI
12 nanosheets of a single pore thickness of 1.5 nm were obtained, which represents
13 less than a single crystal unit-cell dimension (2.0 nm).^[80] Compared to the bulk
14 zeolite, the obtained nanosheets present comparable acidity, thermal and
15 hydrothermal stability. The examples presented up to now strongly indicated the
16 necessity of at least two ammonium headgroups in the surfactant in order to reach
17 hierarchical organized structures.^[28]
18

19 This assumption was counterevidenced by the group of Che^[81] who designed
20 surfactants featuring merely one cationic center able to produce the nanosheets,
21 organized in such a way to form hierarchical assemblies. The authors firstly
22 studied the role of CTAB in the synthesis of MFI type zeolites, which in the
23 appropriate conditions acts as conventional short chain SDA of the MFI structure,
24 in which the surfactant tails are located in the straight channels of the zeolite
25 framework.^[82] The authors suggest that the sole interaction between the
26 surfactant tails is not strong enough to prevent the zeolite crystallization to occur
27 in the conventional way. Based on this evidence, surfactants were rationally
28 designed by ending the surfactant tails with aromatic groups, which enables them
29 to interact through π - π stacking (**Figure 9**). This allowed for the formation of
30 ordered MFI nanosheets, spaced by the surfactant micelles in which center the
31 aromatic groups were located.^[83] Furthermore, they prepared bolaform type
32 surfactants that due their π - π stacking ability proved suitable candidates for the
33 preparation of single crystalline MFI nanosheets, which were assembled through
34 a 90° rotational intergrowth of the sheets. The authors further indicated that single
35 and double-branched ammonium-based surfactants featuring aromatic groups
36 were restricted to direct the synthesis to lamellar nanosheets of the MFI structure
37 (**Figure 9C**). The same group rationalized a new family of surfactants which can
38 be seen as triple branched surfactants where the three branches are connected to a
39 common aromatic center and which branches contain multiple cationic
40
41
42
43
44
45
46
47
48
49
50
51
52
53
54
55
56
57
58
59
60

1
2
3 ammonium groups. Through the use of this surfactant in the synthesis gel, a
4 single crystalline mesoporous ZSM-5 could be achieved featuring intracrystalline
5 slit-like mesoporous arrangements.^[84] The authors reasoned the achievement of
6 this structural feature by dividing the role of the three branches of the surfactant.
7
8 Whilst two of the surfactant branches align within the straight MFI microporous
9 channels, the remaining branch directs the micropores along the zigzag channel.
10
11 The aromatic centers of the surfactant assemble through π - π stacking leading to
12 the development of tailored mesoporosity.
13
14

15
16 The up to now described approaches for the formation of hierarchical structures
17 proved to be of great versatility. A considerable variety of surfactants have been
18 developed up to the point of presenting an entire design concept for the
19 development of mesoporous features (**Figure 10**). Yet, the synthesis of such
20 functional surfactants is often complex and expensive. It is difficult to conceive
21 any commercial application of hierarchical structures described by the above
22 techniques. Furthermore, in most cases aggregation of nanosized zeolites and/or
23 the development of intergrown nanosheets is observed. Indeed, these bottom-up
24 surfactant-oriented approaches do not produce truly zeolite crystals that feature
25 intracrystalline mesoporosity and at the same time intense zeolite crystallinity.
26
27 Nonetheless, these developed strategies have greatly contributed to the
28 comprehension of the interaction of surfactants during zeolite growth.
29
30
31
32
33
34
35
36
37

38 **4. Surfactant-templating strategies through post-synthetic treatment of zeolites**

39 Post-synthetic treatment of zeolites in the presence of surfactants has revealed as a
40 powerful and convenient approach for the development of hierarchical porosity. Two
41 main approaches can be distinguished within the post-synthetic strategies that yield
42 markedly different materials. Hence, a careful consideration of both approaches is
43 critically important. These two strategies have been coined with the terms “zeolite
44 recrystallization” and “zeolite surfactant-templating”. Occasionally, these strategies are
45 mistaken in the literature.^[85] The fundamental difference between the strategies is that
46 whilst in recrystallization the zeolite is exposed to severe basic conditions prior to the
47 addition of the surfactant, in zeolite surfactant-templating the zeolite is treated with a
48 milder basic solution that contain the surfactant (**Figure 11**).
49
50
51
52
53
54
55
56
57
58
59
60

4.1 Zeolite recrystallization in the presence of surfactants: A dissolution and precipitation process

Goto *et al.*^[86] were the first to describe materials achieved through the post-synthetic treatment of various zeolites in basic conditions followed by the addition of surfactants and thermal processing. The authors reported the treatment of zeolites with solutions of different basicities (from 0.75 to 3 M of aqueous NaOH) for a fixed time interval (30 min) prior to the addition of the surfactant (CTAB) and hydrothermal treatment at 150 °C with intermediate pH adjustment to 8.5. Composite materials consisting of a purely mesoporous yet amorphous phase and of the parent zeolite were obtained. The amount of the mesoporous amorphous phase revealed to be dependent on the concentration of the base, as the dissolution of the zeolite was favored at increased pH (**Figure 12**). The authors found striking similarities in the obtained composite materials when MOR and ZSM-5 were used, yet the employment of Al rich zeolites, *i.e.* zeolites with low Si/Al ratios (such as Y and LTA) revealed as unfruitful. Most likely, the high Al content of the zeolite hinders the process. It is important to stress, that whilst the information gathered from nitrogen physisorption and from the XRD does not allow to distinguish between the presence of a truly hierarchical zeolite and a composite material, the SEM images clearly indicate the presence of two phases for the materials prepared by Goto *et al.* (**Figure 12**). The described example illustrates the importance to characterize the materials through complementary techniques that together allow to discriminate between truly hierarchical solids and composites.

Ivanova and co-workers eventually coined the terms “zeolite recrystallization” to refer to this process.^[87] Yet, this denotation is somewhat deceptive as actually a non-crystalline phase is produced as a result of the treatment and therefore there is no real recrystallization. It appears more adequate to refer to a dissolution and re-assembly process. As a function of the severity of the dissolution step, the authors divided the achieved composites into three distinct materials classes (**Figure 11**).^[88,89] The RZEO-1 materials (also described as RMI) are obtained through the treatment of zeolites with mild basic conditions (generally below 1 M) and can be described as partially desilicated zeolite covered by a thin layer of amorphous mesoporous material. Through applying more severe basic conditions; composite materials described as RZEO-2 were achieved. RZEO-3 materials (also named RMII) are achieved through more severe basic

1
2
3 treatments (basic concentrations above 1 M) and can be described as purely amorphous
4 mesoporous aluminosilicates that contain zeolite fragments within the pore walls. It is
5 important to mention that a pH readjustment is required for synthesis where the pH
6 exceeds 12, through the intermediate addition of acid to lower pH values in the range of
7 8 and 10.5 to allow the precipitation of the amorphous phase in the presence of the
8 surfactant. The RZEO materials were extensively studied by *ex situ* MAS NMR and
9 IR. Based on the observations on H-MOR zeolite, Ivanova *et al.*^[90] proposed the
10 following mechanism to account for the formation of the RZEO-1, 2 and 3 materials:

- 11 1) As result of the exposure of the zeolite to the basic solution (NaOH), fast ion
12 exchange between the sodium cations with the zeolite protons and destruction
13 of the silicon-oxygen bonds through alkali are observed, leading to desilication
14 and the formation of large mesopores (3-20 nm) within the crystal and even
15 wider pores in between the crystals.
- 16 2) Owing to the addition of CTAB, the diffusion of surfactant molecules within
17 the inter- and intracrystalline space takes place, leading to ion exchange of the
18 sodium cations with CTA⁺. The surfactants then form micelles inside the in
19 step 1) developed cavities.
- 20 3) The mesophase finally forms through the condensation of the inorganic species
21 dissolved from the zeolite framework in step 1) around the surfactant micelles.

22
23
24
25
26
27
28
29
30
31
32
33
34
35
36 Though the RZEO-3 were described as purely amorphous ordered
37 aluminosilicates featuring no zeolite crystallinity, spectroscopic techniques
38 allowed for evidencing the presence of zeolite subunits within the pore walls that
39 built up the mesoporous structure. The authors ascribed to the presence of these
40 zeolitic fragments within the walls superior hydrothermal stability and enhanced
41 catalytic properties of these materials over Al-MCM-41.^[89,91]

42
43
44
45
46 Boukoussa *et al.*^[92] further described the influence of the amount of employed
47 CTAB on the textural characteristics of the composite materials by using ZSM-5
48 as starting zeolite. Similar conclusions were drawn by Liu *et al.*^[93] using ZSM-
49 22. Na *et al.*^[94] reported the control of the pore size as a function of the chain
50 length of the employed trimethylalkylammonium-based surfactant. The synthesis
51 rout was further applied to TS-1, leading to titanosilicates with mesoporosity of a
52 wider size distribution.^[95]

1
2
3 Solely one article reports the employment of other than
4 trimethylalkylammonium-based surfactants in the zeolite recrystallization
5 process.^[96] Here, mesoporous titanosilicates were achieved by employing the
6 unsymmetrical Gemini surfactant $C_{18}H_{37}Me_2N(CH_2)_6NPr_3Br_2$. A core/shell
7 titanosilicate consisting of a highly crystallized MFI (TS-1) structure both in the
8 core and in the shell yet featuring different framework unit cell long-range
9 extensions was produced (**Figure 13**).

16 **4.2 Zeolite mesostructuring through post-synthetic zeolite surfactant-templating**

17 A post-synthetic surfactant-based strategy allowing for the introduction of
18 mesoporosity within zeolite crystals was firstly reported by Garcia Martinez *et*
19 *al.*,^[97] and later described as mesostructuring to emphasize the precise control
20 over the mesopore size and organization ascribable to the use of surfactants.^[98]
21 This post-synthetic strategy differs substantially from the previously described
22 recrystallization process as it permits for the development of intracrystalline
23 mesoporosity within a wide number of zeolites comprising the FAU, MFI, CHA,
24 *BEA and MOR structures, among others.^[97] The mesostructuring process is
25 rather simple and relies on the treatment of a parent zeolite with cationic
26 surfactants in basic pH conditions.

27 Through comparing the TEM micrographs of the parent and the mesostructured
28 zeolite, the introduction of tailored mesoporosity distributed homogeneously
29 throughout the entire crystal becomes evident (**Figure 14D and E**). This was
30 further proved from the FE-SEM micrographs, which show smooth crystal
31 surface for the parent zeolite whilst the mesostructured zeolite presents abundant
32 mesoporosity (**Figure 14B and C**). Moreover, the crystal morphology of the
33 original zeolite is maintained after the mesostructuring process; it is for this
34 reason that this treatment has been described as pseudomorphic
35 transformation.^[99]

36 A strong evidence of the surfactant-templating effect was obtained through the
37 use of surfactants with increasing aliphatic chain lengths (**Figure 14F and G**).
38 From argon physisorption experiments, an excellent linear correlation between
39 the number of carbon atoms in the surfactant and the achieved mesopores
40 diameter was observed; tailorable in the range from 3.0 to 5.5 nm.^[100]
41
42
43
44
45
46
47
48
49
50
51
52
53
54
55
56
57
58
59
60

1
2
3 Very recently, the development of tailored mesoporosity was observed through *in situ*
4 XRD synchrotron radiation (**Figure 14G**).^[101] This study revealed the gradual evolution
5 of two peaks in the low angle range of the diffractogram corresponding to the formation
6 of the mesoporosity within the zeolite by the surfactant CTAB. These peaks were
7 interpreted through theoretical calculations, revealing the development of short-range
8 ordered mesoporosity. Indeed, through progressively decreasing the size of a zeolite
9 crystal containing hexagonally ordered mesopores, the merging of the corresponding
10 (11) and (20) planes in the simulated diffractograms was observed (**Figure 14H**). It can
11 hence be assumed that the features in the low angle XRD range that develop during
12 surfactant-templating can readily be ascribed to a local hexagonal order of the forming
13 mesoporosity. The theoretical calculations further evidenced a slight decrease of the
14 intensity of the XRD peaks due to a less efficient diffraction caused by the introduction
15 of intracrystalline mesoporosity. This is in agreement to what has been observed
16 experimentally. Furthermore by analyzing the intensity and the FWHM of the XRD
17 peaks it could be evidenced that the mesoporous zeolites present a larger coherent
18 crystal size, which consists of small lattice domains aligned to form part of a single
19 crystal.
20

21 It is important to note that an *in situ* XRD experiment performed in the absence of
22 CTAB shows a very fast decrease of intensity of the zeolite phase (and falls to zero
23 within 10 min of the experiment) whilst no additional peaks could be distinguished in
24 the low angle region. This result hence highlights the striking difference between
25 desilication and zeolite surfactant templating.
26

27 Liquid-Cell Transmission Electron Microscopy (Liq-TEM) has developed to a powerful
28 tool for the *in situ* characterization of processes in materials chemistry.^[102] Liq-TEM
29 was used for the first time in the direct visualization of the changes in the morphology
30 of individual zeolite crystals during surfactant-templating.^[101] The progressive
31 reconstruction of the zeolite crystals could be evidenced by the time-resolved imaging
32 of larger mesopores (due to steaming) present in the parent zeolite (**Figure 14I**).
33

34 These evidences strongly suggest that the development of intracrystalline
35 mesoporosity produces the rearrangement of the zeolite structure (**Figure**
36 **14A**).^[98] Although the exact mechanism of this process is yet not fully
37 understood, it has been suggested that the first stage of the transformation is
38 related with the fast uptake of the cationic surfactant by the zeolite at basic pH.
39 The base reacts with some of Si-O-Si bonds allowing for the fragilization of the
40

1
2
3 structure that rearranges in order to accommodate the forming surfactant micelles
4 within the structure.
5

6 The proposed mechanism does not involve the dissolution and recrystallization of
7 the zeolite species, as misrepresented in some publications,^[85,103] but the short-
8 scale rearrangement of the zeolite framework to accommodate the developing
9 surfactant-micelles. Consequently, the zeolite crystals expand throughout the
10 process as was inferred by measuring crystal sizes from electron microscopy
11 micrographs.^[104]
12

13 The occurrence of desilication or dealumination could be unambiguously
14 discarded through the careful analysis of the filtrates throughout the process and
15 by observing constancy of the Si/Al ratio and of the unit cell size (UCS) of the
16 zeolites during the process. Further, recovery yields of calcined mesostructured
17 zeolites approximate to 100%. This is a further evidence that the employment of
18 the surfactant during the basic treatment prevents any significant dissolution of
19 the zeolite and leads to the mesostructuration. Moreover, it was observed that the
20 employment of small tetraalkylammonium cations (such as
21 tetrapropylammonium hydroxide) preserve the zeolite crystallinity during base
22 treatment, indicating the ability of such cations to preserve from zeolite
23 desilication.^[105] Yet, in these cases no tailored mesoporosity develops due to the
24 inability of these cations to form micelles and hence no surfactant-templating is
25 observed.
26

27 As previously betoken, zeolite phases featuring low Si/Al ratios (*i.e.* Si/Al < 3)
28 are not prone to react in basic conditions as a result of the stability of the Si-O-Al
29 bonds at high pH. To overcome this limitation, Garcia Martinez and co-workers
30 proposed a mild acid pre-treatment, which allows to selectively open some of the
31 Al-O-Si bonds yet without significantly dealuminating the zeolite.^[106] Merely a
32 slight reduction of the UCS of the framework and a small increase in the Si/Al
33 ratio indicated limited removal of Al species from the zeolite structure. For
34 example, the acid treatment applied to a Na-Y zeolite with Si/Al = 2.5, results in
35 the increase to the same ratio to 3.5. This ratio is significantly lower than the
36 elevated Si/Al ratios required by USY and other zeolites (typically Si/Al > 15) for
37 the formation of mesoporosity. Yet, the subsequent surfactant-templating of the
38 acid-treated Na-Y zeolite in the presence of both, the base and CTAB, allows for
39 the introduction of tailored mesoporosity within aluminum-rich zeolites.
40
41
42
43
44
45
46
47
48
49
50
51
52
53
54
55
56
57
58
59
60

1
2
3 Due to the efficiency that surfactant-templating presents for the introduction of
4 tailored mesoporosity within zeolites, Galarneau *et al.*^[107] employed
5 mesostructured zeolites as model structures for assessing the validity of the *t*-plot
6 method. The authors reported that the classically employed *t*-plot approach
7 considerably underestimates microporous volume in hierarchical materials. Based
8 on their observations an abacus for correcting the values obtained from the *t*-plot
9 method was proposed. Ascribable to their well-defined structure, mesoporous
10 zeolites obtained by surfactant-templating can be seen as unique model materials
11 since the size and amount of introduced mesoporosity can readily be tailored.
12 This anticipates their future use as reference materials in a wide variety of fields.
13 Sachse *et al.*^[108] recently employed new surfactants relying on imidazolium and
14 pyridinium based ionic liquids, in the zeolite surfactant-templating process. The
15 authors observed that despite the fact that all of the surfactants present similar
16 templating ability for the formation of ordered mesoporous silica, their
17 employment in zeolite surfactant-templating allows for the achievement of
18 different porous features. Based on this observation the authors suggest that
19 micellization occurs differently in the confined zeolite spaces. These findings are
20 a further proof that fosters the rearrangement mechanism.^[98]
21
22
23
24
25
26
27
28
29
30
31
32
33

34 **5. Key characteristics of mesostructured zeolites required for industrial** 35 **applications**

36
37 The development of mesoporosity in zeolites is driven by the quest for
38 overcoming their diffusion limitations in many industrially relevant catalytic
39 processes. In order to understand to which extent the main zeolite properties are
40 affected upon introducing mesoporosity the in-depth characterization of various
41 key features is essential; these are: (i) the textural properties of the mesoporous
42 zeolites, including the pore size and porous architecture, (ii) the crystallinity, (iii)
43 the density, strength and nature of the acid sites and (iv) the hydrothermal
44 stability. The assessment of these key properties is critically important to assert
45 the suitability of mesoporous zeolites for large scale applications. In order to
46 diligently describe these key features a variety of advanced characterization
47 techniques are being developed and are becoming available. Some of the latest
48 evolutions in this field have recently been reviewed by Perez-Ramirez and co-
49 workers.^[109]
50
51
52
53
54
55
56
57
58
59
60

5.1 Textural and diffusional properties

The full textural characterization of hierarchical zeolites comprises a detailed quantitative and qualitative appreciation of their porous architecture and porous interconnectivity at different length scales. The by far most widespread characterization technique for analyzing the porosity of hierarchical zeolites is nitrogen physisorption. Yet, nitrogen features a quadrupole moment, which implies that its molecular orientation strongly depends on the surface chemistry of the adsorbent. This leads to the major inconvenience of high uncertainty of its molecular cross-sectional area. Moreover, the presence of the quadrupole moment strongly affects the micropore filling pressure, which in some cases renders the measurement of equilibrated adsorption isotherms difficult. Additionally, the nitrogen molecule can hinder the pore entrances of small micropores through pre-adsorption, which makes the estimation of the micropore size distribution difficult.^[110] In this respect, argon physisorption techniques present important advantages. Argon features a smaller kinetic diameter and no quadrupole moment, weaker fluid-wall interactions and a higher adsorption temperature compared to nitrogen. These characteristics reduce diffusion limitations and allow for observing the micropore filling at higher relative pressures compared to nitrogen for zeolites.^[111]

Moreover, measuring Ar isotherms at lower temperatures than its boiling temperature (*e.g.* 77 or 65 K) allows to gain structural insights in the porous features of mesoporous zeolites. Recording Ar isotherms at such low temperatures influences the thermodynamic state of the confined fluid and allows for the observation of hysteresis even for very small mesopores (below 4 nm). This is of crucial importance for mesoporous zeolites that feature small mesopores, where nitrogen physisorption reveals a reversible capillary condensation step. In a recent paper, Ar isotherms were recorded at 77 and 65 K for surfactant-templated USY zeolite. A combination of H1 and H2 hysteresis was observed, indicating that the majority of the mesopores are freely accessible without constriction (H1 loop). The part of the hysteresis related to the H2 loop is due to mesopores accessible through the narrow microporous channels, *i.e.* mesopores imbedded in the zeolite crystal; which leads to the cavitation phenomena (**Figure 15**).^[112] A confirmation of this observation was gathered by analysis of hysteresis scanning measurements, where the pore system was

1
2
3 partially filled up to defined partial pressures. By performing several cycles
4 through adsorbing various amounts of adsorbate, the presence of cavitation was
5 unambiguously assessed as the scanning curves returned directly to the
6 desorption boundary curve. The combination of these two techniques allowed for
7
8 quantifying the amount of accessible and constricted mesoporosity in the
9 mesostructured USY zeolites and amounted to 64 and 36%, respectively for the
10 material presenting a total mesoporous volume of $0.23 \text{ cm}^3 \text{ g}^{-1}$. It has been argued
11 that the presence of the constricted mesoporosity accounts as proof of the
12 rearrangement process in which the diffusion of individual surfactant molecules
13 within the microporous network and their subsequent self-assembly lead to the
14 formation of mesoporosity within the zeolite crystals. It is important to mention,
15 that longer surfactant-templating treatment times, yield materials which isotherms
16 do not present the H2 loop, indicating that if enough time is allowed for the
17 mesopore formation to occur all of the mesopores are accessible from the exterior
18 of the crystal.
19

20
21
22
23
24
25
26
27
28
29
30
31
32
33
34
35
36
37
38
39
40
41
42
43
44
45
46
47
48
49
50
51
52
53
54
55
56
57
58
59
60
Microscopy techniques are undoubtedly one of the major tools allowing for the
study of porosity at different length scales. Novel visualization techniques
become ever more available for the detailed description of the porous features in
hierarchical zeolites. One example hereof is electron tomography, allowing for
the study of mesopore connectivity in zeolites.^[113] For deeper insights to these
techniques the reader is oriented to consult the excellent review by Wei *at al.*^[114]
that summarizes the existing visualization methods with special focus on the
determination on the interconnectivity between the porosities.

The unique hierarchical and intracrystalline nature of the mesopores in surfactant-
templated zeolites was recently visualized though the combination of electron
diffraction and microscopy studies by employing two advanced characterization
techniques, *i.e.* electron tomography (ET) and rotation electron diffraction (RED).^[115]
The combination of these techniques features the paramount advantage of overcoming
the limitations of electron tomography (which does not permit for resolving the zeolite
microporosity), as the RED method provides 3D structural information at the atomic
level.^[116] Hence, the combination of these two techniques allowed for the
unprecedented description and direct visualization of the porous architecture of the
hierarchical zeolite from the atomic to the mesoscale (**Figure 16**). This allowed for the
illustration of the porous architecture and of the mesoporous connectivity through the

1
2
3 reconstructed model.^[117] The development of this technique has indeed been described
4 as major advancement for the characterization of hierarchical crystalline solids.^[118] Here
5 it allowed to unambiguously proof the crystallinity of the mesoporous zeolites and to
6 discard the presence of any mesoporous amorphous material in the surfactant-templated
7 material.
8

9
10
11 In addition to the textural characterization of hierarchical zeolites, the assessment
12 of the impact of the porosity on the diffusion properties of the materials is of
13 paramount importance. Galarneau *et al.*^[119] recently reported the study of mass-
14 transfer properties of post-synthetic surfactant-templated USY zeolite by pulsed
15 field gradient nuclear magnetic resonance (PFG NMR). The authors compared
16 the transport phenomena in USY zeolite, in surfactant-templated USY and in a
17 mechanical mixtures of USY zeolite and Al-MCM-41 (**Figure 17**). Diffusion in
18 the mechanical mixture could be described as a superimposition of the transport
19 properties of the microporous zeolite and mesoporous solid. Differently, the
20 effective diffusivity obtained for the surfactant-templated zeolite proved to be
21 intermediate between that for the zeolite and the one observed for the mesoporous
22 material and inferior to the one achieved in the mechanical mixture. This set of
23 data not only proves the interconnectivity of the micro- (zeolitic) and
24 mesoporosity (surfactant-templated) in one single phase but further that the
25 hierarchical structure is effective in improving the diffusion properties of greatly
26 hampered microporous solids. In addition, these results discard the formation of
27 composite materials (mechanical mixture) through surfactant-templating as
28 previously suggested.^[85,103]
29
30
31
32
33
34
35
36
37
38
39
40
41
42

43 **5.2 Acidity**

44 The employed strategy for the formation of mesoporosity within the zeolites can
45 have an important impact on the acid sites as their electronic environment may
46 vary compared to the sites in the bulk zeolite. This is typically observed for
47 hierarchical zeolites that are prepared through destructive techniques such as
48 desilication.^[120] These strategies affect greatly the Si/Al ratio and further lead to
49 defects in the structure as well as to partial amorphization of the material. This
50 results in a substantial increase of Lewis acidity to the expense of Brønsted
51 acidity and alters thus the acid characteristics of the parent zeolites.^[121]
52
53
54
55
56
57
58
59
60

1
2
3 The post-synthetic surfactant-templating process does not present this
4 inconvenient due to the employment of mild basic conditions and the protective
5 role of the surfactant, allowing to maintain the acidic properties of the zeolites in
6 a very unique manner while introducing a significant amount of mesoporosity.^[98]
7
8 Various techniques have been developed to quantitatively and qualitatively assess
9 the acidity of hierarchical zeolites, which are generally based on the adsorption of
10 probe molecules. One of the most widely employed methods to determine the
11 total acidity of zeolites is temperature programmed desorption of ammonia (TPD-
12 NH₃). Yet, this method has been argued of not being accurate, as in many cases,
13 adsorption on non-acid sites and re-adsorption of the probe molecule during the
14 temperature treatment can readily occur, which makes it difficult to compare
15 TPD-NH₃ profiles of bulk and hierarchical zeolites.^[122] Despite, Chal *et al.*
16 compared the TPD-NH₃ profiles of USY zeolite and of mesostructured USY
17 through surfactant-templating, finding very similar global acidity in both samples
18 (**Figure 18A**).^[99]

19
20 A more comprehensive assessment of the acidity in zeolites is given through
21 infrared spectroscopy.^[123] Indeed, through identifying characteristic vibrational
22 bands it is possible to follow the development of silanol groups during the
23 surfactant-templating process (**Figure 18B**).^[98] In pristine NH₄-Y zeolite, two
24 bands at 3640 and 3740 cm⁻¹ are observed, characteristic for the vibrational
25 frequencies of strong Brønsted acid Si-(OH)-Al bonds and silanol Si-OH bonds,
26 respectively. After the acid treatment, the band centered at 3740 cm⁻¹ increases
27 substantially whereas the band at 3640 cm⁻¹ decreases. This observation indicates
28 the formation of new terminal silanol groups (sometimes also referred as
29 hydroxyl nest) confirming the partial opening of the Si-O-Al bonds. Upon
30 surfactant-templating, the 3640 cm⁻¹ band significantly decreases which can be
31 explained through the exchange of protons by CTA⁺ and Na⁺. Through surfactant
32 removal and exchange with NH₄⁺, Brønsted acidity is then recovered. The
33 selective opening of the Si-O-Al bonds was also proved through ²⁷Al MAS NMR
34 (**Figure 18C**). Here, the sole observation of tetrahedral Al indicates the absence
35 of the formation of extraframework Al species throughout the entire process.^[98]

36
37 One of the most suited techniques for the quantitative analysis of acid sites in
38 zeolites is pyridine titration through the assignment of modes of the pyridine ions
39 formed at Brønsted acid sites (1544 cm⁻¹) and coordination complexes formed at
40
41
42
43
44
45
46
47
48
49
50
51
52
53
54
55
56
57
58
59
60

1
2
3 Lewis acid sites (1455 cm^{-1}). This technique was used to analyze the impact of
4 the introduction of mesoporosity through surfactant-templating on USY zeolite.
5 The pyridine adsorption followed by infrared spectroscopy indicated the presence
6 of Brønsted and Lewis acidity for both, parent USY and surfactant-templated
7 USY. It is quite remarkable that the introduction of a large amount of
8 mesoporosity ($0.41 \text{ cm}^3 \text{ g}^{-1}$) within USY zeolite almost did not affect the acidic
9 properties of the zeolite. Whilst the concentration of Brønsted sites diminished
10 slightly for desorption temperature at $150 \text{ }^\circ\text{C}$ (from 0.28 to 0.23 mmol g^{-1}), the
11 concentration of Lewis acid sites remained constant (0.08 mmol g^{-1}). At
12 desorption temperatures of $350 \text{ }^\circ\text{C}$ equal concentration of Lewis and Brønsted
13 acid sites within both materials were determined (0.06 and 0.15 mmol g^{-1}),
14 indicating that the strongest acid sites remain unaffected through surfactant-
15 templating (**Figure 18D**).
16
17
18
19
20
21
22
23
24
25

26 **5.3 Hydrothermal stability**

27 Hydrothermal stability is an important key characteristic especially relevant for
28 industrial applications, as the presence of steam at elevated temperature is
29 common in industrial processes. The rapid loss of structural integrity is indeed
30 one of the major drawbacks surfactant-templated silica-aluminas (such as Al-
31 MCM-41) present, making their industrial application impractical.^[124] Corma
32 stated in his introductory 1997 review: “A strong improvement in stability could
33 be obtained if one could make the walls crystalline. If this could be achieved one
34 can dream of producing materials not only more stable and with stronger acidities
35 than the current MCM-41 but also having in the same structure a combination of
36 well-defined micro- and mesopores.” In this respect, the development of
37 intracrystalline mesoporosity within zeolites through surfactant-templating
38 represents the achievement of this long lasting goal and allows the bridging of the
39 gap between MCM-41 and zeolites.^[104]
40
41
42
43
44
45
46
47
48
49

50 In order to assess the hydrothermal stability of mesostructured USY zeolite, its texture
51 and crystallinity were compared before and after deactivation by steaming. To this
52 purpose, their nitrogen isotherms and the X-ray diffractograms were compared at
53 different steps during the preparation and after the deactivation (**Figure 19**). The
54 nitrogen isotherm of the mesostructured Y zeolite featured a typical sharp nitrogen
55 uptake at a relative pressure of approximately 0.5 as a result of the filling of surfactant-
56
57
58
59
60

1
2
3 templated mesoporosity. Through the additional ultrastabilization process - that
4 converts the mesostructured Y zeolite in mesostructured USY zeolite - the mesopores
5 size became wider. Yet, the total mesoporosity remained almost constant. The
6 deactivation of mesostructured USY zeolite simulating the process occurring in a FCC
7 unit was achieved through treating the mesostructured USY at 788 °C in pure steam for
8 4 h. Though the mesoporous size distribution became wider throughout the treatment,
9 its mesoporous volume kept constant, confirming excellent hydrothermal stability of the
10 mesostructured zeolite.^[98]

11
12
13
14
15
16 In the next section we will describe the impact of the mesostructured Y zeolite in
17 fluid catalytic cracking (FCC). Proceeding to this, we would like to highlight that
18 the excellent hydrothermal stability of the mesostructured zeolite was confirmed
19 in month-long commercial FCC trials in a North American refinery.^[125] Hereto,
20 the evolution of the zeolite surface area (ZSA, calculated through the *t*-plot
21 method) and the mesoporous surface area (MSA, also called matrix surface area
22 in industry; as the matrix accounts for a significant fraction of the mesopore
23 surface area of the FCC catalyst it is calculated by subtracting the ZSA from the
24 BET area) was monitored throughout the trial through periodic sampling of the
25 equilibrium catalyst (**Figure 19C**). It was inferred that the ZSA of the
26 equilibrium catalyst increased from 115 to 123 m² g⁻¹ (+ 7%), as a result of
27 slightly higher ZSA in the fresh surfactant-templated zeolite. At the same time, an
28 important increase in the MSA of the equilibrium catalysts, from 30 m² g⁻¹ before
29 the trial to 50 m² g⁻¹ (+ 70%) towards the end of the trial was observed. The
30 chemical analysis of the equilibrium catalysts further revealed the presence of
31 1000 ppm of vanadium and 200 ppm of nickel in the equilibrium catalysts. The
32 presence of vanadium is known to harm FCC catalysts through the formation of
33 vanadic acid, which forms through hydrothermal conditions present in the FCC
34 unit. Notwithstanding, it was evidenced that the activity of the catalyst remained
35 constant as to before of the trial through Micro Activity Tests (MAT). The
36 excellent hydrothermal stability of the surfactant-templated USY, confirmed both
37 in the lab and in the refinery, is an additional evidence of the presence of
38 intracrystalline mesoporosity and discard the suggested amorphous nature of the
39 mesoporous phase, as this would not stand the severe hydrothermal conditions
40 applied.
41
42
43
44
45
46
47
48
49
50
51
52
53
54
55
56
57
58
59
60

6. Mesoporous zeolites in fluid catalytic cracking (FCC) and refining applications

Zeolites play a central role in the petrochemical industry, being the main component of catalysts used in the processing of hydrocarbons through cracking, hydrocracking, isomerization and aromatization reactions, among many others. Especially the big five zeolite family (which comprises the phases Y, ZSM-5, FER, MOR and *BEA) presents unique properties such as strong Brønsted acidity, large surface area and hydrothermal stability, rendering them especially prone for these applications.

Activity, selectivity and deactivation are the key parameters that determine the efficiency of a catalytic process. All of them are crucially influenced by the mass-transfer properties of the zeolite. A variety of catalytic test reactions have been established with the aim to assess the role of the secondary porosity in hierarchical zeolites. Many of the established test reactions are of industrial interest and comprise both the transformation of hydrocarbons and the production of chemicals, such as the methanol to olefins reaction and the Friedel-Crafts alkylation, just to cite a few examples. Hartmann *et al.*^[126] recently reviewed frequently employed test reactions that allow to determine the effect of secondary porosity in zeolites on their catalytic efficiency. Commonly, the employment of hierarchical zeolites affects the catalytic properties by (i) improving conversion of bulky molecules, (ii) enhancing selectivity by avoiding secondary reactions (as a result of shorter diffusion path length) and (iii) reducing catalyst deactivation.

The role of intracrystalline mesoporosity on the catalytic activity and selectivity of hierarchical zeolites will here be exemplified through the application surfactant-templated USY in catalytic cracking. This represents the first example of an industrial application of a hierarchical zeolite moreover in a very demanding and important process such as fluid catalytic cracking (FCC).^[100]

FCC is a key process in the petroleum refinery industry, which allows for transforming the high boiling point high molecular weight hydrocarbons present in the crude oil into lighter and more valuable fractions such as diesel, gasoline and olefinic gases. For a thorough introduction to FCC the reader is referred to the specialized literature.^[127,128]

The main component of the FCC catalyst is zeolite Y as it is responsible for most of the catalytic cracking due to its unique structure, featuring 3D interconnected micropores, and to its strong acidity. Yet, a significant fraction of the reactant

1
2
3 molecules in the feedstock are of larger size than the microporous channels of
4 this zeolite.^[129] Consequently, mass-transfer is importantly hampered as solely
5 the active sites located on the external surface of the zeolite crystals are able to
6 transform the bulky molecules. The effect of diffusion limitations on the product
7 distribution in FCC is schematically depicted in the simplified tree-lump model
8 (**Figure 20A**). Under such conditions less vacuum gas oil (VGO) is converted
9 into gasoline and light cycle oil (LCO) due to the accessibility issues. At the same
10 time, as a result of the long diffusion path lengths in the bulk zeolites, secondary
11 reactions occur (overcracking), which increases the selectivity towards undesired
12 gases and coke.

13
14 To overcome this scenario, an important amount of work has been carried out
15 with the aim to reduce the diffusion path length and to increase the number of
16 accessible active sites in zeolites. It has indeed been reported that through
17 employing nanosized zeolites, the selectivity towards reaction intermediates (*i.e.*
18 gasoline and LCO) was increased whilst reducing the production of gases and
19 coke.^[130] The achieved selectivity can be explained by taking into account the
20 reduced diffusion path length in the nanosized zeolites, as the reaction
21 intermediates, *i.e.* gasoline and LCO, reside less time within the crystalline
22 structure and are thus less prone to undergo secondary reactions (*i.e.*
23 overcracking) to form undesired gases and coke which deactivates the
24 catalyst.^[131]

25
26 Despite the increased selectivity towards the gasoline fraction in FCC for which
27 nanocrystalline Y zeolite accounts, several important drawbacks render their
28 industrial application difficult. These are based on the low yield of the
29 nanocrystals and their rather complex separation after synthesis. Additionally,
30 such nanocrystals present lower hydrothermal stability than the bulk zeolites.^[131]

31
32 A practical alternative for reducing the diffusion path length and at the same time
33 maximizing the accessibility of active sites – and which does not present the
34 afore mentioned drawbacks - is the introduction of mesoporosity within zeolite Y.
35 As previously described, mesoporous zeolite Y obtained through post-synthetic
36 surfactant-templating presents excellent acidity and hydrothermal stability and at
37 the same time tailored and interconnected mesoporosity. These features endow
38 the mesostructured Y zeolite as ideal component of the FCC catalyst.

1
2
3 For this purpose, the FCC catalyst was produced employing commercial
4 techniques and tools at a pilot plant.^[100] Bulk NH₄-Y zeolite was treated with a
5 diluted citric acid solution in order to selectively open some of the Si-O-Al
6 bonds. The sample was subsequently surfactant-templated to introduce tailored
7 mesoporosity. The in this way achieved mesostructured Y zeolite was
8 ultrastabilized by exposing it to 550 °C during 2 h in 100% steam. In order to
9 further improve its hydrothermal stability, the mesostructured USY zeolite was
10 rare earth ion exchanged. Finally, it was combined with clay (kaoline) acting as
11 filler and a binder (aluminium chlorohydrol) and shaped into the FCC catalyst
12 through spray drying. In order to simulate the equilibrium catalyst (Ecat), the
13 achieved catalyst was deactivated through fluidized steaming at 788 °C during 8 h
14 in 100% steam.^[125]

15
16
17
18
19
20
21
22
23 The catalytic performance of the FCC catalyst containing the mesostructured
24 zeolite Y was compared to a system prepared in identical manner but comprising
25 the original Y zeolite. The FCC tests were carried out in an advanced cracking
26 evaluation (ACE) unit using both light and heavy VGO as feedstock. In both
27 cases, higher yields in gasoline and LCO were observed whilst at the same time
28 significantly less coke and bottoms (unconverted feed) were produced when
29 using the mesoporous containing FCC catalyst (**Figure 21**). The selectivity
30 towards gasoline and LCO was even better when employing heavy VGO. These
31 results highlight the role of intracrystalline mesoporosity in zeolites in increasing
32 the accessibility of the feedstock molecules to the active sites – which is
33 evidenced by the more effective conversion of the bottom especially for heavy
34 VGO (**Figure 21C**) - and in facilitating the ready exit of the intermediates that
35 leads to a significant decrease in the production of coke and an increase of
36 gasoline and LCO. The increased selectivity towards intermediates (gasoline and
37 LCO) is a clear evidence of the role of shorter diffusion path length in reducing
38 overcracking reactions (**Figure 20B**).

39
40
41
42
43
44
45
46
47
48
49 A more realistic description of the various conversions occurring during FCC is
50 given by the six-lump model (**Figure 22**). Here the conversion of VGO to the
51 different fractions is modeled as a series of parallel and consecutive reactions. In
52 FCC, all light products can be formed directly from the VGO, yet their formation
53 from secondary reaction is also significant.^[132] The shortening of the diffusion
54 path length allows for minimizing the occurrence of secondary reactions and thus
55
56
57
58
59
60

1
2
3 increasing the yield of the desired gasoline and LCO. The model furthermore
4 depicts liquefied petroleum gas (LPG), which is an important fraction of the FCC
5 process. LPG consists of light paraffins (propane and butane) and olefins
6 (propylene and butylene). Whilst olefins represent valuable FCC products, being
7 the starting material for many other transformations, paraffins represent products
8 with rather low economic interest. Indeed, maximizing propylene production has
9 become a major issue in FCC due to an increasing demand/supply imbalance,
10 although different markets have different needs at different times.^[133]

11
12 During the FCC process, olefins transform through hydrogen transfer reaction
13 into the corresponding paraffins. In order to prevent the hydrogen transfer
14 reaction to occur, the residence time of the olefins inside the catalyst must be
15 reduced for example by shortening of the diffusion path length. In a commercial
16 operation in a refinery,^[134] a steady increase in LPG olifinicity was observed
17 through replacing the incumbent FCC catalyst by another containing the
18 mesostructured Y zeolite. Commercial data confirmed the observed trend using
19 an equilibrium catalyst from the refinery and analyzed in an ACE unit (**Figure**
20 **23A**). A gradual increase in the LPG olefinicity was also observed at the refinery
21 as the concentration of the FCC catalyst containing mesostructured Y zeolite in
22 the circulating inventory steadily increased (**Figure 23B**). In this commercial
23 trial, the most important yield shift was the increase in butylene selectivity
24 (**Figure 23C**). Furthermore, a very valuable increase in gasoline octane was also
25 observed due to a higher concentration of olefins in the lighter gasoline fraction
26 (**Figure 23D**).

27
28 A different commercial trial was carried out at Alon's Big Spring, TX refinery, in which
29 318 tons of the equilibrium FCC catalyst comprising mesostructured USY zeolite
30 produced by Grace using Rive Technology surfactant-templating technology.^[135] The
31 catalyst addition to the FCC unit was of 3 tons/day, which represents the equivalent
32 amount as for the incumbent catalyst. As a result of the improved bottom cracking
33 ability of the FCC catalyst containing the mesostructured zeolite, the operation
34 conditions of the refinery were allowed to be modified through lowering the riser
35 temperature whilst at the same time increasing the feed throughput (**Figure 24A**).
36 Consequently, a decrease in the temperature of the regenerator was induced, which yet
37 did not affect the regeneration of the catalyst. Throughout the trial the combination of
38 improved coke selectivity whilst increasing feed rate allowed to achieve a significant
39
40
41
42
43
44
45
46
47
48
49
50
51
52
53
54
55
56
57
58
59
60

1
2
3 increase in both gasoline (**Figure 24B**) and LCO production (**Figure 24C**). The
4 observed selectivity towards intermediates confirms that the introduction of
5 intracrystalline mesoporosity shortens the diffusion path length and hinders the
6 occurrence of secondary reactions. At the end of the commercial trial, the additional
7 value that was delivered to the refinery by replacing the incumbent catalyst with the
8 mesostructured USY containing FCC catalyst was estimated to be over US\$2.50/bbl of
9 the FCC feed (**Figure 24D**). This value is well above the catalytic uplift estimated from
10 extensive preliminary testing using an ACE unit (US\$ 2.00/bbl of FCC feed). Sampling
11 of the equilibrium catalyst during the entire duration of the trial, allowed to assess the
12 excellent mechanical and hydrothermal stability of the catalyst containing
13 mesostructured Y zeolite.^[136]

14
15
16
17
18
19
20
21 Several thousand tons of FCC catalyst featuring mesostructured USY zeolite have
22 up to date been produced. The elevated cost of the surfactant-based process could
23 be overcome through improving employed raw materials and operating
24 conditions, which allowed to decrease manufacturing cost by a factor of ten
25 during the up-scaling process. Moreover, it has been shown that the cost of the
26 surfactant-templating process can be substantially minimized by recovering and
27 recycling the surfactant.^[137]

28
29
30
31
32
33 Building on the successful commercialization of surfactant-templating
34 technology for FCC, new hierarchical zeolites are being produced using this
35 strategy to meet the needs of the refinery industry by providing more flexibility
36 and improved performance in a rapidly changing environment. On this regard, the
37 joint effort between Zeolyst International, CRI/Criterion Inc and Rive
38 Technology for the commercialization of surfactant-templated zeolites as superior
39 hydrocracking catalysts is a major step towards expanding this technology to new
40 refining processes. Currently, surfactant-templated zeolites based on other
41 structures such as ZSM-5, beta, mordenite and chabazite, among others, are being
42 tested in refining, petrochemical and fine chemical applications.

43 44 45 46 47 48 49 50 51 **7. Further perspectives and concluding remarks**

52
53 An impressive variety of surfactant-oriented techniques has emerged in the last
54 few years to design complex mesoporous architectures within a wide range of
55 materials. Specifically, the use of surfactant-oriented strategies for the fabrication
56 of mesoporous zeolites has allowed to overcome the drawbacks related with the
57
58
59
60

1
2
3 limited accessibility to the active sites of purely microporous zeolites. However,
4 the development of mesoporous zeolites using surfactants is still at an early stage.
5 Although, surfactant-oriented strategies allow for the preparation of hierarchical
6 zeolites with interconnected porosity at different length scales, the control over
7 their porous architecture is much poorer than in the case of amorphous solids.
8 The quest remains opened for the synthesis of hierarchical zeolites featuring
9 mesopores arranged in different geometries.

10
11 As this and other challenges are being tackled by several groups, an exciting new
12 opportunity opens with the use of surfactant-oriented strategies for the formation
13 of tailored mesoporosity in other microporous materials. Indeed, surfactant-
14 templating strategies have lately been adapted for the development of
15 mesoporosity in MOFs through careful choosing of the conditions of co-assembly
16 of the surfactants and the individual MOF building units.^[17] The mesoporous
17 MOFs obtained using this strategy are very promising materials for gas storage,
18 as the introduction of secondary porosity within MOFs allows for the acceleration
19 of the adsorption kinetics and increases the overall storage capacity for bulkier
20 molecules. In the particular, the application of surfactant-oriented strategies for
21 the development of mesoporous zinc imidazolate frameworks (ZIFs) have
22 recently proven successful.^[138] Those structures are especially interesting, as
23 some of their structural types are isomorphic to zeolite structures.

24
25 The development of new synthetic strategies to produce tailored mesoporosity in
26 zeolites that are at the same time inexpensive and eco-friendly is very much
27 needed. The use of natural surfactants and biopolymers and the recycling of the
28 surfactant are anticipated to play a major role in overcoming the current
29 constraints.

30
31 The introduction of mesoporosity in zeolites is an effective way to influence the
32 diffusion properties of these microporous solids. However, a more detailed
33 understanding on the impact of the secondary porosity in the mass transport
34 properties of the zeolites is critical as they greatly influence key aspects of
35 heterogeneous catalysis, such as activity, selectivity and catalyst lifetime. Various
36 techniques are used to investigate mass transport phenomena in porous materials,
37 such as invert gas and zero length column chromatography and pulse field
38 gradient NMR (PFG-NMR).^[139] Unfortunately, diffusion studies are not
39 standardized, which makes cross comparisons very problematic.

1
2
3 Recent advances in visualization techniques are allowing for a better analysis of
4 the location and interconnectivity of porosity in zeolites at different length scales.
5 Specially, Environmental-TEM has been used to follow *in-situ* the transformation
6 of the secondary porosity in zeolites during surfactant-templating in USY,
7 providing valuable insights on the formation mechanism.^[101]

8
9
10 A better understanding on both, how surfactants produce mesoporosity in zeolites
11 and the role of this in the diffusion properties of hierarchical zeolites, is essential
12 for the rational design of new materials with improved properties. One of the
13 field that can benefit from more accessible strong acid solid catalysts is the
14 transformation of biomass into high value chemicals and fuels. For example,
15 valuable oxygenated chemicals, such as furans, aldehydes, ketones have been
16 obtained using zeolites with strong acidity and large mesopores in the
17 transformation of very abundant but very bulky and highly recalcitrant lignin.^[140]
18 Moreover, mesoporous zeolites are promising in fields other than catalysis, such
19 as in water treatment, gas separation, and as sensors.^[141] Finally, new
20 developments in the adsorption and transformation of CO₂ by functionalized
21 mesoporous zeolites reveal that the modification of the surface chemistry of
22 zeolite, for example via grafting, could play a very important role in the
23 future.^[142]

24
25
26 Whilst the introduction of mesoporosity in zeolites present important advantages
27 for a wide number of applications,^[143] the industrialization of these materials is
28 still in an early stage. However, the commercialization of surfactant-templated
29 zeolites in FCC is expected to foster the development of new hierarchical zeolites
30 and their use both in existing processes and new and exciting opportunities.

31 32 33 **Acknowledgements**

34
35
36 The authors acknowledge the EU and MINECO through the CAPITA Project
37 WAVES (EP7-NMP- 266543 and PCIN-2013-175) and FEDER - for financial
38 support.

39 40 41 **References**

- 42
43
44 [1] V. Chiola, J. E. Ritsko and C. D. Vanderpool, Process for Producing Low-
45 bulk Density Silica, US Patent 3,556, 725, 1971.

- 1
2
3 [2] F. Di Renzo, H. Cambon, R. Dutartre, A 28-Year-Old Synthesis of Micelle-
4 templated Mesoporous Silica, *Microporous Mater.* **1997**, *10*, 283-286.
5
6 [3] T. Yanagisawa, T. Shimizu, K. Kuroda, C. Kato, The Preparation of
7 Alkyltriethylammonium–Kaneinite Complexes and Their Conversion to
8 Microporous Materials, *Bull. Chem. Soc. Jpn.* **1990**, *63*, 988-992.
9
10 [4] J. S. Beck, C. T.-W. Chu, I. D. Johnson, C. T. Kresge, M. E. Leonowicz, W.
11 J. Roth, J. W. Vartuli, Synthetic Porous Crystalline Material: its Synthesis
12 and Use WO Patent 91/11390, **1991**.
13
14 [5] C. T. Kresge, M. E. Leonowicz, W. J. Roth, J. C. Vartuli, J. S. Beck,
15 Ordered Mesoporous Molecular Sieves Synthesized by a Liquid-Crystal
16 Template Mechanism, *Nature*, **1992**, *359*, 710-712.
17
18 [6] J. S. Beck, J. C. Vartuli, W. J. Roth, M. E. Leonowicz, C. T. Kresge, K. D.
19 Schmitt, C. T. W. Chu, D. H. Olson, E. W. Sheppard, S. B. McCullen, J. B.
20 Higgins, J. L. Schlenker, A New Family of Mesoporous Molecular Sieves
21 Prepared with Liquid Crystal Templates, *J. Am. Chem. Soc.* **1992**, *114*,
22 10834-10843.
23
24 [7] J. Y. Ying, C. P. Mehnert, M. S. Wong, Synthesis and Applications of
25 Supramolecular□Templated Mesoporous Materials, *Angew. Chem. Int. Ed.*
26 **1999**, *38*, 56-77.
27
28 [8] Y. Shi, Y. Wan, D. Zhao, Ordered Mesoporous Non-Oxide Materials,
29 *Chem. Soc. Rev.* **2011**, *40*, 3854-3878.
30
31 [9] Y. Wan, D. Zhao, On the Controllable Soft-templating Approach to
32 Mesoporous Silicates, *Chem. Rev.* **2007**, *107*, 2821-2860.
33
34 [10] Q. Huo, D. I. Margolese, U. Ciesla, P. Feng, T. E. Gier, P. Sieger, R. Leon,
35 P. M. Petroff, F. Schüth, G. D. Stucky, Generalized Synthesis of Periodic
36 Surfactant/Inorganic Composite Materials, *Nature* **1994**, *368*, 317-321.
37
38 [11] G. J. A. A. Soler-Illia, C. Sanchez, B. Lebeau, J. Patarin, Chemical
39 Strategies to Design Textured Materials: from Microporous and Mesoporous
40 Oxides to Nanonetworks and Hierarchical Structures, *Chem. Rev.* **2002**, *102*,
41 4093-4138.
42
43 [12] Q. Huo, D. I. Margolese, G. D. Stucky, Surfactant Control of Phases in the
44 Synthesis of Mesoporous Silica-Based Materials, *Chem. Mater.* **1996**, *8*,
45 1147-1160.
46
47
48
49
50
51
52
53
54
55
56
57
58
59
60

- 1
2
3 [13] J. Man Kim, Y. Sakamoto, Y. Kyu Hwang, Y.-U. Kwon, O. Terasaki, S.-E.
4 Park, G. D. Stucky, Structural Design of Mesoporous Silica by Micelle-
5 Packing Control using Blends of Amphiphilic Block Copolymers, *J. Phys.*
6 *Chem. B* **2002**, *106*, 2552-2558.
7
8
9 [14] A. Blanz, S. P. Armes, A. J. Ryan, Self-Assembled Block Copolymer
10 Aggregates: from Micelles to Vesicles and Their Biological Applications,
11 *Macromol. Rapid Commun.* **2009**, *30*, 267-277.
12
13 [15] T.-Y. Ma, L. Liu, Z.-Y. Yuan, Direct Synthesis of Ordered Mesoporous
14 Carbons, *Chem. Soc. Rev.* **2013**, *42*, 3977-4003.
15
16 [16] L.-G. Qui, T. Xu, Z.-Q. Li, W. Wang, Y. Wu, X. Jiang, X.-Y. Tian, L.-D.
17 Zhang, Hierarchically Micro- and Mesoporous Metal–Organic Frameworks
18 with Tunable Porosity, *Angew. Chem. Int. Ed.* **2008**, *47*, 9629-9633.
19
20 [17] D. Bradshaw, S. El-Hankari, L. Lupica-Spagnolo, Supramolecular
21 Templating of Hierarchically Porous Metal–Organic Frameworks, *Chem.*
22 *Soc. Rev.* **2014**, *43*, 5431-5443.
23
24 [18] K. Cassiers, T. Linssen, M. Mathieu, M. Benjelloun, K. Schrijnemakers, P.
25 Van Der Voort, P. Cool, E. F. Vansant, A Detailed Study of Thermal,
26 Hydrothermal, and Mechanical Stabilities of a Wide Range of Surfactant
27 Assembled Mesoporous Silicas, *Chem. Mater.* **2002**, *14*, 2317-2324.
28
29 [19] A. Corma. From Microporous to Mesoporous Molecular Sieve Materials and
30 their Use in Catalysis, *Chem. Rev.* **1997**, *97*, 2373-2420.
31
32 [20] K. R. Kloestra, H. van Bekkum, J. C. Jansen, Mesoporous Material
33 Containing Framework Tectosilicate by Pore–Wall Recrystallization, *Chem.*
34 *Commun.* **1997**, 2281-2282.
35
36 [21] M. J. Verhoef, P. J. Kooyman, J. C. van der Waal, M. S. Rigutto, J. A.
37 Peters, H. van Bekkum, Partial Transformation of MCM-41 Material into
38 Zeolites: Formation of Nanosized MFI Type Crystallites, *Chem. Mater.*
39 **2001**, *13*, 683-687.
40
41 [22] K. Schumacher, P. I. Ravikovitch, A. Du Chesne, A. V. Neimark, K. K.
42 Unger, Characterization of MCM-48 Materials, *Langmuir* **2000**, *16*, 4648-
43 4654.
44
45 [23] Y. Fang, H. Hu, An Ordered Mesoporous Aluminosilicate with Completely
46 Crystalline Zeolite Wall Structure, *J. Am. Chem. Soc.* **2006**, *128*, 10636-
47 10637.
48
49
50
51
52
53
54
55
56
57
58
59
60

- 1
2
3 [24] J. Garcia Martinez, K. Li (Eds.), *Mesoporous Zeolites: Preparation,*
4 *Characterization and Application*, Wiley, **2015**.
5
6 [25] J. Perez-Ramirez, C. H. Christensen, K. Egeblad, C. H. Christensen, J. C.
7 Groen, Hierarchical Zeolites: Enhanced Utilisation of Microporous Crystals
8 in Catalysis by Advances in Materials Design, *Chem. Soc. Rev.* **2008**, *37*,
9 2530-2542.
10
11 [26] W. J. Roth, P. Nachtigall, R. E. Morris, J. Čejka, Two-Dimensional Zeolites:
12 Current Status and Perspectives, *Chem. Rev.* **2014**, *114*, 4807-4837.
13
14 [27] M. V. Opanasenko, W. J. Rothab, J. Čejka, Two-Dimensional Zeolites in
15 Catalysis: Current Status and Perspectives, *Catal. Sci. Technol.* **2016**, *6*,
16 2467-2484.
17
18 [28] K. Möller, T. Bein, Mesoporosity—A New Dimension for Zeolites, *Chem.*
19 *Soc. Rev.* **2013**, *42*, 3689-3707.
20
21 [29] D. P. Serrano, J. M. Escola, P. Pizarro, Synthesis Strategies in the Search for
22 Hierarchical Zeolites, *Chem. Soc. Rev.* **2013**, *42*, 4004-4035.
23
24 [30] S. Lopez-Orozco, A. Inayat, A. Schwab, T. Selvam, W. Schwieger, Zeolitic
25 Materials with Hierarchical Porous Structures, *Adv. Mater.* **2011**, *23*, 2602-
26 2615.
27
28 [31] C. J. H. Jacobsen, C. Madsen, J. Houzvicka, I. Schmidt, A. Carlsson,
29 Mesoporous Zeolite Single Crystals, *J. Am. Chem. Soc.* **2000**, *122*, 7116-
30 7117.
31
32 [32] R. Chal, C. Gérardin, M. Bulut, S. van Donk, Overview and Industrial
33 Assessment of Synthesis Strategies towards Zeolites with Mesopores,
34 *ChemCatChem* **2011**, *3*, 67-81.
35
36 [33] K. R. Kloetstra, H. W. Zandbergen, J. C. Jansen, H. van Bekkum,
37 Overgrowth of Mesoporous MCM-41 on Faujasite, *Microporous Mater.*
38 **1996**, *6*, 287-293.
39
40 [34] A. Karlsson, M. Stocker, R. Schmidt, Composites of Micro-and Mesoporous
41 Materials: Simultaneous Syntheses of MFI/MCM-41 Like Phases by a
42 Mixed Template Approach, *Micropor. Mesopor. Mater.* **1999**, *27*, 181-192.
43
44 [35] S. Du, F. Li, Q. Sun, N. Wang, M. Jia, J. Yu, A Green Surfactant-Assisted
45 Synthesis of Hierarchical TS-1 Zeolites with Excellent Catalytic Properties
46 for Oxidative Desulfurization, *Chem. Commun.* **2016**, *52*, 3368-3371.
47
48
49
50
51
52
53
54
55
56
57
58
59
60

- 1
2
3 [36] J. Zhu, Y. Zhu, L. Zhu, M. Rigutto, A. van der Made, C. Yang, S. Pan, L.
4 Wang, L. Zhu, Y. Jin, Q. Sun, Q. Wu, X. Meng, D. Zhang, Y. Han, J. Li, Y.
5 Chu, A. Zheng, S. Qiu, X. Zheng, F.-S. Xiao, Highly Mesoporous Single-
6 Crystalline Zeolite Beta Synthesized Using a Nonsurfactant Cationic
7 Polymer as a Dual-Function Template, *J. Am. Chem. Soc.* **2014**, *136*, 2503-
8 2510.
- 9
10
11
12 [37] F.-S. Xiao, L. Wang, C. Yin, K. Lin, Y. Di, J. Li, R. Xu, D. S. Su, R.
13 Schlögl, T. Yokoi, T. Tatsumi, Catalytic Properties of Hierarchical
14 Mesoporous Zeolites Templated with a Mixture of Small Organic
15 Ammonium Salts and Mesoscale Cationic Polymers, *Angew. Chem. Int. Ed.*
16 **2006**, *118*, 3162-3165.
- 17
18
19 [38] F. Liu, T. Willhammar, L. Wang, L. Zhu, Q. Sun, X. Meng, W. Carrillo-
20 Cabrera, X. Zou, F.-S. Xiao, ZSM-5 Zeolite Single Crystals with B-Axis-
21 Aligned Mesoporous Channels as an Efficient Catalyst for Conversion of
22 Bulky Organic Molecules, *J. Am. Chem. Soc.* **2012**, *134*, 4557-4560.
- 23
24
25 [39] J.-Y. Liu, J.-G. Wang, N. Li, H. Zhao, H.-J. Zhou, P.-C. Sun, T.-H. Chen,
26 Polyelectrolyte–Surfactant Complex as a Template for the Synthesis of
27 Zeolites with Intracrystalline Mesopores, *Langmuir* **2012**, *28*, 8600-8607.
- 28
29 [40] H. Wang, T. J. Pinnavaia, MFI Zeolite with Small and Uniform Intracrystal
30 Mesopores, *Angew. Chem. Int. Ed.* **2006**, *45*, 7603-7606.
- 31
32 [41] S. R. Stojkovic, B. Adnadjevic, Investigation of the NaA Zeolite
33 Crystallization Mechanism by IR Spectroscopy, *Zeolites* **1988**, *6*, 523-525.
- 34
35 [42] Y. Liu, W.Z. Zhang, T. J. Pinnavaia, Steam-Stable Aluminosilicate
36 Mesostructures Assembled from Zeolite Type Y Seeds, *J. Am. Chem. Soc.*
37 **2000**, *122*, 8791-8792.
- 38
39 [43] Y. Liu, W. Zhang, T. J. Pinnavaia, Steam-Stable MSU-S Aluminosilicate
40 Mesostructures Assembled from Zeolite ZSM-5 and Zeolite Beta Seeds,
41 *Angew. Chem. Int. Ed.* **2001**, *40*, 1255-1258.
- 42
43 [44] Z. Zhang, Y. Han, F.-S. Xiao, S. Qiu, L. Zhu, R. Wang, Y. Yu, Z. Zhang, B.
44 Zou, Y. Wang, H. Sun, D. Zhao, Y. Wei, Mesoporous Aluminosilicates with
45 Ordered Hexagonal Structure, Strong Acidity, and Extraordinary
46 Hydrothermal Stability at High Temperatures, *J. Am. Chem. Soc.* **2001**, *123*,
47 5014-5021.
- 48
49
50
51
52
53
54
55
56
57
58
59
60

- 1
2
3 [45] Z. Zhang, Y. Han, L. Zhu, R. Wang, Y. Yu, S. Qiu, D. Zhao, F.-Shou Xiao,
4 Strongly Acidic and High-Temperature Hydrothermally Stable Mesoporous
5 Aluminosilicates with Ordered Hexagonal Structure, *Angew. Chem. Int. Ed.*
6 **2001**, *40*, 1258-1262.
7
8
9 [46] P. Li, G. Xiong, L. Liu, L. Wang, Investigation on the Effect of Zeolite
10 Precursor on the Formation Process of MCM-41 Containing Zeolite Y
11 Building Units, *Spectrochim. Acta Mol. Biomol. Spectrosc.* **2013**, *107*, 218-
12 226.
13
14 [47] P. Li, L. P. Liu, G. Xiong, Effect of Zeolite Precursor on the Formation of
15 MCM-41 Molecular Sieve Containing Zeolite Y Building Units, *Phys.*
16 *Chem. Chem. Phys.* **2011**, *13*, 11248-11253.
17
18 [48] Y. Liu, T. J. Pinnavaia, Metakaolin as a Reagent for the Assembly of
19 Mesoporous Aluminosilicates with Hexagonal, Cubic and Wormhole
20 Framework Structures from Proto-Faujasitic Nanoclusters, *J. Mater. Chem.*
21 **2004**, *14*, 3416-3420.
22
23 [49] Q. Huo, R. Leon, P. M. Petroff, G. D. Stucky, Mesostructure Design with
24 Gemini Surfactants: Supercage Formation in a Three-Dimensional
25 Hexagonal Array, *Science* **1995**, *268*, 1324-1327.
26
27 [50] Y. Liu, T. J. Pinnavaia, Assembly of Hydrothermally Stable Aluminosilicate
28 Foams and Large-Pore Hexagonal Mesostructures from Zeolite Seeds under
29 Strongly Acidic Conditions, *Chem. Mater.* **2002**, *14*, 3-5.
30
31 [51] D. H. Park, S.-S. Kim, T. J. Pinnavaia, F. Tzompantzi, J. Prince, J. S.
32 Valente, Selective Isobutene Oligomerization by Mesoporous MSU-SBEA
33 Catalysts, *J. Phys. Chem. C* **2011**, *115*, 5809-5816.
34
35 [52] F. N. Gu, F. Wei, J. Y. Yang, N. Lin, W. G. Lin, Y. Wang, J. H. Zhu, New
36 Strategy to Synthesis of Hierarchical Mesoporous Zeolites, *Chem. Mater.*
37 **2010**, *22*, 2442-2450.
38
39 [53] Y. Zhu, Z. Hua, J. Zhou, L. Wang, J. Zhao, Y. Gong, W. Wu, M. Ruan, J.
40 Shi, Hierarchical Mesoporous Zeolites: Direct Self-Assembly Synthesis in
41 a Conventional Surfactant Solution by Kinetic Control over the Zeolite Seed
42 Formation, *Chem. Eur. J.* **2011**, *17*, 14618-14627.
43
44 [54] X. Zhou, H. Chen, Y. Zhu, Y. Song, Y. Chen, Y. Wang, Y. Gong, G. Zhang,
45 Z. Shu, X. Cui, J. Zhao, J. Shi, Dual-Mesoporous ZSM-5 Zeolite with
46
47
48
49
50
51
52
53
54
55
56
57
58
59
60

- 1
2
3 Highly b-Axis-Oriented Large Mesopore Channels for the Production of
4 Benzoin Ethyl Ether, *Chem. Eur. J.* **2013**, *19*, 10017-10023.
- 5
6 [55] A. Sachse, C. Wuttke, E. Lissner, M. O. de Souza, Ordered Mesoporous
7 ZSM-5 Employing an Imidazolium-Based Ionic Liquid, *Chem. Eur. J.*
8 **2014**, *20*, 14996-14999.
- 9
10 [56] T. Wang, H. Kaper, M. Antonietti, B. Smarsly, Templating Behavior of a
11 Long-Chain Ionic Liquid in the Hydrothermal Synthesis of Mesoporous
12 Silica, *Langmuir* **2007**, *23*, 1489-1495.
- 13
14 [57] S. Liu, X. Cao, L. Li, C. Li, Y. Ji, F.-S. Xiao, Preformed Zeolite Precursor
15 Route for Synthesis of Mesoporous X Zeolite, *Colloids Surf. A* **2008**, *318*,
16 269-274.
- 17
18 [58] J. Song, L. Ren, C. Yin, Y. Ji, Z. Wu, J. Li, F.-S. Xiao, Stable, Porous, and
19 Bulky Particles with High External Surface and Large Pore Volume from
20 Self-Assembly of Zeolite Nanocrystals with Cationic Polymer, *J. Phys.*
21 *Chem. C* **2008**, *112*, 8609-8613.
- 22
23 [59] M. Thommes, B. Smarsly, M. Groenewolt, P. I. Ravikovits, A. V. Neimark,
24 Adsorption Hysteresis of Nitrogen and Argon in Pore Networks and
25 Characterization of Novel Micro- and Mesoporous Silicas, *Langmuir* **2006**,
26 *22*, 756-764.
- 27
28 [60] D. P. Serrano, J. Aguado, J. M. Escola, J. M. Rodriguez, A. Peral,
29 Hierarchical Zeolites with Enhanced Textural and Catalytic Properties
30 Synthesized from Organofunctionalized Seeds, *Chem. Mater.* **2006**, *18*,
31 2462-2464.
- 32
33 [61] D. P. Serrano, J. Aguado, G. Morales, J. M. Rodriguez, A. Peral, M.
34 Thommes, J. D. Epping, B. F. Chmelka, Molecular and Meso- and
35 Macroscopic Properties of Hierarchical Nanocrystalline ZSM-5 Zeolite
36 Prepared by Seed Silanization, *Chem. Mater.* **2009**, *21*, 641-654.
- 37
38 [62] J. Aguado, D. P. Serrano, J. M. Rodriguez, Zeolite Beta with Hierarchical
39 Porosity Prepared from Organofunctionalized Seeds, *Micropor. Mesopor.*
40 *Mater.* **2008**, *115*, 504-513.
- 41
42 [63] H. Zhang, L. Wang, D. Zhang, X. Meng, F.-S. Xiao, Mesoporous and Al-
43 Rich MFI Crystals Assembled with Aligned Nanorods in the Absence of
44 Organic Templates, *Microporous Mesoporous Mater.* **2016**, *233*, 133-139.
- 45
46
47
48
49
50
51
52
53
54
55
56
57
58
59
60

- 1
2
3 [64] M. Choi, H. S. Cho, R. Srivastava, C. Venkatesan, D.-H. Choi, R. Ryoo,
4 Amphiphilic Organosilane-Directed Synthesis of Crystalline Zeolite with
5 Tunable Mesoporosity, *Nature Mater.* **2006**, *5*, 718-723.
6
7 [65] K. Cho, R. Ryoo, S. Asahina, C. Xiao, M. Klingstedt, A. Umemura, M. W.
8 Anderson, O. Terasaki, Mesopore Generation by Organosilane Surfactant
9 During LTA Zeolite Crystallization, Investigated by High-Resolution SEM
10 and Monte Carlo Simulation, *Solid State Sci.* **2011**, *13*, 750-756.
11
12 [66] G. V. Shanbhag, M. Choi, J. Kim, R. Ryoo, Mesoporous Sodalite: A Novel,
13 Stable Solid Catalyst for Base-Catalyzed Organic Transformations, *J. Catal.*
14 **2009**, *264*, 88-92.
15
16 [67] M. Choi, R. Srivastava, R. Ryoo, Organosilane Surfactant-Directed
17 Synthesis of Mesoporous Aluminophosphates Constructed with Crystalline
18 Microporous Frameworks, *Chem. Commun.* **2006**, 4380-4382.
19
20 [68] A. Inayat, I. Knoke, E. Spiecker, W. Schwieger, Assemblies of Mesoporous
21 FAU-Type Zeolite Nanosheets, *Angew. Chem. Int. Ed.* **2012**, *51*, 1962-
22 1965.
23
24 [69] M. Qamar, I. Baig, A.-M. Azad, M. I. Ahmed, M. Qamaruddin, Synthesis of
25 Mesoporous Zeolite Y Nanocrystals in Octahedral Motifs Mediated by
26 Amphiphilic Organosilane Surfactant, *Chem. Eng. J.* **2016**, *290*, 282-289.
27
28 [70] K. Cho, H. S. Cho, L.-C. de Ménorval, R. Ryoo, Generation of Mesoporosity
29 in LTA Zeolites by Organosilane Surfactant for Rapid Molecular Transport
30 in Catalytic Application, *Chem. Mater.* **2009**, *21*, 5664-5673.
31
32 [71] J. Han, D. Liu, Creation of Mesopores in ZSM-5 Zeolite Crystals by a Novel
33 Double-acyloxy Organosilane Surfactant, *Chem. Lett.* **2015**, *44*, 992-994.
34
35 [72] J. Han, D. Liu, Influence of Synthesis Conditions on the Mesopore
36 Distribution and Morphology Control of Hierarchical ZSM-5 Zeolites
37 Synthesized by Double-Acyloxy Organosilane Surfactants, *Eur. J. Inorg.*
38 *Chem.* **2015**, 5081-5088.
39
40 [73] M. Choi, K. Na, J. Kim, Y. Sakamoto, O. Terasaki, R. Ryoo, Stable Single-
41 Unit-Cell Nanosheets of Zeolite MFI as Active and Long-Lived Catalysts,
42 *Nature* **2009**, *461*, 246-249.
43
44 [74] K. Na, M. Choi, W. Park, Y. Sakamoto, O. Terasaki, R. Ryoo, Pillared MFI
45 Zeolite Nanosheets of a Single-Unit-Cell Thickness, *J. Am. Chem. Soc.*
46 **2010**, *132*, 4169-4177.
47
48
49
50
51
52
53
54
55
56
57
58
59
60

- 1
2
3 [75] R. J. Messinger, K. Na, Y. Seo, R. Ryoo, B. F. Chmelka, Co-development
4 of Crystalline and Mesoscopic Order in Mesostructured Zeolite Nanosheets,
5 *Angew. Chem. Int. Ed.* **2015**, *54*, 927-931.
6
7 [76] B. Liu, K. Xie, S. C. Oh, D. Sun, Y. Fang, H. Xi, Direct Synthesis of
8 Hierarchical USY Zeolite for Retardation of Catalyst Deactivation, *Chem.*
9 *Eng. Sci.* **2016**, *153*, 374-381.
10
11 [77] C. Li, Y. Ren, J. Gou, B. Liu, H. Xi, Facile Synthesis of Mesostructured
12 ZSM-5 Zeolite with Enhanced Mass Transport and Catalytic Performances,
13 *Appl. Surf. Sci.* **2017**, *392*, 785-794.
14
15 [78] K. Na, C. Jo, J. Kim, K. Cho, J. Jung, Y. Seo, R. J. Messinger, B. F.
16 Chmelka, R. Ryoo, Directing Zeolite Structures into Hierarchically
17 Nanoporous Architectures, *Science* **2011**, *333*, 328-332.
18
19 [79] L. Wu, V. Degirmenci, P. C. M. M. Magusin, B. M. Szyja, E. J. M. Hensen,
20 Dual Template Synthesis of a Highly Mesoporous SSZ-13 Zeolite with
21 Improved Stability in the Methanol-to-Olefins Reaction, *Chem. Commun.*
22 **2012**, *48*, 9492-9494.
23
24 [80] J. Jung, C. Jo, K. Cho, R. Ryoo, Zeolite Nanosheet of a Single-Pore
25 Thickness Generated by a Zeolite-Structure-Directing Surfactant, *J. Mater.*
26 *Chem.* **2012**, *22*, 4637-4640.
27
28 [81] D. Xu, S. Che, O. Terasaki, A Design Concept of Amphiphilic Molecules
29 for Directing Hierarchical Porous Zeolite, *New J. Chem.* **2016**, *40*, 3982-
30 3992.
31
32 [82] D. Xu, J. Feng, S. Che, An Insight into the Role of the Surfactant CTAB in
33 the Formation of Microporous Molecular Sieves, *Dalton Trans.* **2014**, *43*,
34 3612-3617.
35
36 [83] D. Xu, Y. Ma, Z. Jing, L. Han, B. Singh, J. Feng, X. Shen, F. Cao, P.
37 Oleynikov, H. Sun, O. Terasaki, S. Che, π - π Interaction of Aromatic Groups
38 in Amphiphilic Molecules Directing for Single-crystalline Mesostructured
39 Zeolite Nanosheets, *Nature Commun.* **2014**, *5*, 4262-427.
40
41 [84] B. K. Singh, D. Xu, L. Han, J. Ding, Y. Wang, S. Che, Synthesis of Single-
42 crystalline Mesoporous ZSM-5 with Three-dimensional Pores via the Self-
43 Assembly of a Designed Triply Branched Cationic Surfactant, *Chem. Mater.*
44 **2014**, *26*, 7183-7188.
45
46
47
48
49
50
51
52
53
54
55
56
57
58
59
60

- 1
2
3 [85] D. Verboekend, N. Nuttens, R. Locus, J. Van Aelst, P. Verolme, J. C. Groen,
4 J. Perez-Ramirez, B. F. Sels, Synthesis, Characterisation, and Catalytic
5 Evaluation of Hierarchical Faujasite Zeolites: Milestones, Challenges, and
6 Future Directions, *Chem. Soc. Rev.* **2016**, *45*, 3331-3352.
7
8
9 [86] Y. Goto, Y. Fukushima, P. Ratu, Y. Imada, Y. Kubota, Y. Sugi, M. Ogura,
10 M. Matsukata, Mesoporous Material from Zeolite, *J. Porous Mater.* **2002**, *9*,
11 43-48.
12
13 [87] I. I. Ivanova, A. S. Kuznetsov, V. V. Yuschenko, E. E. Knyazeva, Design of
14 composite micro/mesoporous molecular sieve catalysts, *Pure Appl. Chem.*
15 **2004**, *76*, 1647-1657.
16
17 [88] I. A. Kasyanova, A. A. Maerle, I. I. Ivanova, V. I. Zaikovskii, Towards
18 Understanding of the Mechanism of Stepwise Zeolite Recrystallization into
19 Micro/Mesoporous Materials, *J. Mater. Chem. A* **2014**, *2*, 16978-16988.
20
21 [89] I. I. Ivanova, E. E. Knyazeva, Micro–Mesoporous Materials Obtained by
22 Zeolite Recrystallization: Synthesis, Characterization and Catalytic
23 Applications, *Chem. Soc. Rev.* **2013**, *42*, 3671-3688.
24
25 [90] I. I. Ivanova, I. A. Kasyanov, A. A. Maerle, V. I. Zaikovskii, Mechanistic
26 Study of Zeolites Recrystallization into Micro-Mesoporous Materials,
27 *Microporous Mesoporous Mater.* **2014**, *189*, 163-172.
28
29 [91] V. V. Ordonskii, Y. V. Monakhova, E. E. Knyazeva, N. S. Nesterenko, I. I.
30 Ivanova, The Physicochemical Properties of Micro/Mesoporous Materials
31 Prepared by the Recrystallization of Zeolite BEA, *Russ. J. Phys. Chem. A*
32 **2009**, *83*, 1012-1017.
33
34 [92] B. Boukoussa, N. Aouad, R. Hamacha, A. Bengueddach, Key Factor
35 Affecting the Structural and Textural Properties of ZSM-5/MCM-41
36 Composite, *J. Phys. Chem. Sol.* **2015**, *78*, 78-83.
37
38 [93] S. Liu, J. Ren, H. Zhang, E. Lv, Y. Yang, Y.-W. Li, Synthesis,
39 Characterization and Isomerization Performance of Micro/Mesoporous
40 Materials Based on H-ZSM-22 Zeolite, *J. Catal.* **2016**, *335*, 11-23.
41
42 [94] J. Na, G. Liu, T. Zhou, G. Ding, S. Hu, L. Wang, Synthesis and Catalytic
43 Performance of ZSM-5/MCM-41 Zeolites with Varying Mesopore Size by
44 Surfactant-directed Recrystallization, *Catal. Lett.* **2013**, *143*, 267-275.
45
46
47
48
49
50
51
52
53
54
55
56
57
58
59
60

- 1
2
3 [95] N. Wilde, M. Pelz, S. G. Gebhardt, R. Gläse, Highly Efficient Nano-sized
4 TS-1 with Micro-/Mesoporosity from Desilication and Recrystallization for
5 the Epoxidation of Biodiesel with H₂O₂, *Green Chem.* **2015**, *17*, 3378-3389.
6
7 [96] C.-G. Li, Y. Lu, H. Wu, P. Wu, M. He, A Hierarchically Core/Shell-
8 Structured Titanosilicate with Multiple Mesopore Systems for Highly
9 Efficient Epoxidation of Alkenes, *Chem. Commun.* **2015**, *51*, 14905-14908.
10
11 [97] J. Y. Ying, J. Garcia-Martinez, US Patent, Mesostructured Zeolitic
12 Materials and Methods of Making and Using the Same, US20070244347
13 A1, **2005**.
14
15 [98] J. Garcia-Martinez, M. Johnson, J. Valla, K. Li, J. Y. Ying, Mesostructured
16 Zeolite Y - High Hydrothermal Stability and Superior FCC Catalytic
17 Performance, *Catal. Sci. Technol.* **2012**, *2*, 987-994.
18
19 [99] R. Chal, T. Cacciaguerra, S. van Donk, C. Gérardin, Pseudomorphic
20 Synthesis of Mesoporous Zeolite Y Crystals, *Chem. Commun.* **2010**, *46*,
21 7840-7842.
22
23 [100] K. Li, J. Valla, J. Garcia Martinez, Realizing the Commercial Potential of
24 Hierarchical Zeolites: New Opportunities in Catalytic Cracking,
25 *ChemCatChem* **2014**, *6*, 46-66.
26
27 [101] N. Linares, A. Sachse, E. Serrano, A. Grau-Atienza, E. Oliveira Jardim, J.
28 Silvestre-Albero, M. A. Liuthevicene Cordeiro, F. Fauth, G. Beobide, O.
29 Castillo, J. García-Martínez, In Situ Time-Resolved Observation of the
30 Development of Intracrystalline Mesoporosity in USY Zeolite, *Chem.*
31 *Mater.* **2016**, *28*, 8971-8979.
32
33 [102] J. Wu, H. Shan, W. Chen, X. Gu, P. Tao, C. Song, W. Shang, T. Deng, In
34 Situ Environmental TEM in Imaging Gas and Liquid Phase Chemical
35 Reactions for Materials Research, *Adv. Mater.* **2016**, *28*, 9686-9712.
36
37 [103] D. Verboekend, M. Milina, S. Mitchell, J. Perez-Ramirez, Hierarchical
38 Zeolites by Desilication: Occurrence and Catalytic Impact of
39 Recrystallization and Restructuring, *Cryst. Growth Des.* **2013**, *13*, 5025-
40 5035.
41
42 [104] T. Prasomsri, W. Jiao, S. Z. Weng, J. Garcia Martinez, Mesostructured
43 Zeolites: Bridging the Gap between Zeolites and MCM-41, *Chem. Commun.*
44 **2015**, *51*, 8900-8911.
45
46
47
48
49
50
51
52
53
54
55
56
57
58
59
60

- 1
2
3 [105] M. S. Holm, M. K. Hansen, C. H. Christensen, "One-Pot" Ion-Exchange and
4 Mesopore Formation During Desilication, *Eur. J. Inorg. Chem.* **2009**, 1194-
5 1198.
6
7
8 [106] J. Garcia-Martinez, M. M. Johnson, I. Valla, Introduction of Mesoporosity
9 in Low Si/Al Zeolites, US patent, 20100196263, **2010**.
10
11 [107] A. Galarneau, F. Villemot, J. Rodriguez, F. Fajula, B. Coasne, Validity of
12 the T-plot Method to Assess Microporosity in Hierarchical
13 Micro/Mesoporous Materials, *Langmuir* **2014**, *30*, 13266-14274.
14
15 [108] A. Sachse, C. Wuttke, U. Díaz, M. Oberson de Souza, Mesoporous Y
16 Zeolite through Ionic Liquid Based Surfactant Templating, *Micropor.*
17 *Mesopor. Mater.* **2015**, *217*, 81-86.
18
19 [109] S. Mitchell, A. B. Pinar, J. Kevin, P. Crivelli, J. Kräger, J. Perez-Ramirez,
20 Structural Analysis of Hierarchically Organized Zeolites, *Nature Commun.*
21 **2015**, *6*, 8633-8647.
22
23 [110] M. Thommes, K. Kaneko, A. V. Neimark, J. P. Olivier, F. Rodriguez-
24 Reinoso, J. Rouquerol, K. S. W. Sing, Physisorption of Gases, with Special
25 Reference to the Evaluation of Surface Area and Pore Size Distribution,
26 *Pure Appl. Chem.* **2015**, *87*, 1051-1069.
27
28 [111] M. Thommes, K. A. Cychoz, Physical Adsorption Characterization of
29 Nanoporous Materials: Progress and Challenges, *Adsorption* **2014**, *20*, 233-
30 250.
31
32 [112] C. J. Rasmussen, A. Vishnyakov, M. Thommes, B. M. Smarsly, F. Kleitz, A.
33 V. Neimark, Cavitation in Metastable Liquid Nitrogen Confined to
34 Nanoscale Pores, *Langmuir* **2010**, *26*, 10147-10157.
35
36 [113] J. Zecevic, C. J. Gommers, H. Friedrich, P. E. de Jongh, K. P. de Jong,
37 Mesoporosity of Zeolite Y: Quantitative Three-Dimensional Study by
38 Image Analysis of Electron Tomograms, *Angew. Chem. Int. Ed.* **2012**, *51*,
39 4213-4217.
40
41 [114] Y. Wei, T. E. Parmentier, K. P. de Jong, J. Zecevic, Tailoring and
42 Visualizing the Pore Architecture of Hierarchical Zeolites, *Chem. Soc. Rev.*
43 **2015**, *44*, 7234-7261.
44
45 [115] W. Wan, J. Sun, J. Su, S. Hovmoller, X. Zou, Three-dimensional Rotation
46 Electron Diffraction: Software RED for Automated Data Collection and
47 Data Processing, *J. Appl. Crystallogr.* **2013**, *46*, 1863-1873.
48
49
50
51
52
53
54
55
56
57
58
59
60

- 1
2
3 [116] T. Willhammar, Y. Yun, X. Zou, Structural Determination of Ordered
4 Porous Solids by Electron Crystallography, *Adv. Funct. Mater.* **2014**, *24*,
5 182-199.
6
7
8 [117] J. M. Thomas, R. K. Leary, A Major Advance in Characterizing Nanoporous
9 Solids Using a Complementary Triad of Existing Techniques, *Angew. Chem.*
10 *Int. Ed.* **2014**, *53*, 12020-12021.
11
12 [118] J. Garcia-Martinez, C. Xiao, K.A. Cychosz, K. Li, W. Wan, X. Zou, M.
13 Thommes, Evidence of Intracrystalline Mesostructured Porosity in Zeolites
14 by Advanced Gas Sorption, Electron Tomography and Rotation Electron
15 Diffraction, *ChemCatChem* **2014**, *6*, 3110-3115.
16
17 [119] A. Galarneau, F. Guenneau, A. Gedeon, D. Mereib, J. Rodriguez, F. Fajula,
18 B. Coasne, Probing Interconnectivity in Hierarchical
19 Microporous/Mesoporous Materials Using Adsorption and Nuclear
20 Magnetic Resonance Diffusion, *J. Phys. Chem. C* **2016**, *120*, 1562-1569.
21
22 [120] D. Verboekend, J. Pérez-Ramírez, Design of Hierarchical Zeolite Catalysts
23 by Desilication, *Catal. Sci. Technol.* **2011**, *1*, 879-890.
24
25 [121] S. Mitchell, M. Milina, R. Verel, M. Hernandez-Rodriguez, A. B. Pinar, L.
26 B. McCusker, J. Perez-Ramirez, Aluminum Redistribution during the
27 Preparation of Hierarchical Zeolites by Desilication, *Chem. Eur. J.* **2015**, *21*,
28 14156-14164.
29
30 [122] R. J. Gorte, What do we Know about the Acidity of Solid Acids?, *Catal.*
31 *Lett.* **1999**, *62*, 1-13.
32
33 [123] W. E. Farneth, R. J. Gorte, Methods for Characterizing Zeolite Acidity,
34 *Chem. Rev.* **1995**, *95*, 615-635.
35
36 [124] A. Corma, M. S. Grande, V. Gonzalez-Alfaro, A. V. Orchilles, Cracking
37 Activity and Hydrothermal Stability of MCM-41 and its Comparison with
38 Amorphous Silica-Alumina and a USY Zeolite, *J. Catal.* **1996**, *159*, 375-
39 382.
40
41 [125] J. Garcia Martinez, K. Li, G. Krishnaiah, A Mesostructured Y Zeolite as a
42 Superior FCC Catalyst – From Lab to Refinery, *Chem. Commun.* **2012**, *48*,
43 11841-11843.
44
45 [126] M. Hartmann A. G. Machoke, W. Schwieger, Catalytic Test Reactions for
46 the Evaluation of Hierarchical Zeolites, *Chem. Soc. Rev.* **2016**, *45*, 3313-
47 3390.
48
49
50
51
52
53
54
55
56
57
58
59
60

- 1
2
3 [127] W. Vermeiren, J.-P. Gilson, Impact of Zeolites on the Petroleum and
4 Petrochemical Industry, *Top. Catal.* **2009**, *52*, 1131-1161.
5
6 [128] E. T. C. Vogt, B. M. Weckhuysen, Fluid Catalytic Cracking: Recent
7 Developments on the Grand Old Lady of Zeolite Catalysis, *Chem. Soc. Rev.*
8 **2015**, *44*, 7342-7370.
9
10 [129] M. A. Cambor, A. Corma, A. Martinez, F. A. Mocholi, J. Perez Pariente,
11 Catalytic Cracking of Gasoil: Benefits in Activity and Selectivity of Small Y
12 Zeolite Crystallites Stabilized by a Higher Silicon-to-Aluminium Ratio by
13 Synthesis, *Appl. Catal.* **1989**, *55*, 65-74.
14
15 [130] A. Corma, Transformation of Hydrocarbons on Zeolite Catalysts, *Catal.*
16 *Lett.* **1993**, *22*, 33-52.
17
18 [131] K. Rajagopalan, A. W. Peters, G. C. Edwards, Influence of Zeolite Particle
19 Size on Selectivity during Fluid Catalytic Cracking, *Appl. Catal.* **1986**, *23*,
20 69-80.
21
22 [132] M. Heydari, H. AleEbrahim, B. Dabir, Study of Seven-lump Kinetic Model
23 in the Fluid Catalytic Cracking Unit, *Am. J. Appl. Sci.* **2010**, *7*, 71-76.
24
25 [133] A. Akah, M. Al-Ghrami, Maximizing Propylene Production via FCC
26 Technology, *Appl. Petrochem. Res.* **2015**, *5*, 377-392.
27
28 [134] A. Humphries, C. Cooper, J. Seidel, *Increasing Butylenes Production from*
29 *the FCC Unit through Rive's Molecular HighwayTM Technology*, AM-15-32.
30
31 [135] G. Krishnaiah, B. Speronello, A. Hansen, J. Crosby, *American Fuels and*
32 *Petrochemical Manufacturers Annual Meeting*, San Antonio, TX, **2013**.
33
34 [136] B. Speronello, J. Garcia-Martinez, A. Hansen R. Hu, FCC Catalysts with
35 Mesoporous Zeolite Yield Higher Quality Products, *Refin. Oper.* **2011**, *2*, 1-
36 13.
37
38 [137] J. Garcia Martinez, M. Johnson, Methods of Recovery of Pore-forming
39 Agents for Mesoporous Materials, US Patent US8206498, **2012**.
40
41 [138] E. A. Flügel, M. T. Aronson, S. C. Junggeburth, B. F. Chmelka, B. V.
42 Lotsch, Surfactant-directed syntheses of mesoporous zinc imidazolates:
43 formation mechanism and structural insights, *CrystEngComm* **2015**, *17*, 463-
44 470.
45
46 [139] J. Kärger, D. M. Ruthven, D. N. Theodorou, *Diffusion in Nanoporous*
47 *Materials*, Wiley, **2012**.
48
49
50
51
52
53
54
55
56
57
58
59
60

- 1
2
3 [140] C. Li, X. Zhao, A. Wang, G. W. Huber, T. Zhang, Catalytic Transformation
4 of Lignin for the Production of Chemicals and Fuels, *Chem. Rev.* **2015**, *115*,
5 11559-11624.
6
7
8 [141] T. H. Nguyen, H. Gong, S. S. Lee, T.-H. Bae, Amine-Appended
9 Hierarchical Ca-A Zeolite for Enhancing CO₂/CH₄ Selectivity of Mixed-
10 Matrix Membranes, *ChemPhysChem* **2016**, *17*, 3165-3169.
11
12 [142] T. H. Nguyen, S. Kim, M. Yoon, T.-H. Bae, Hierarchical Zeolites with
13 Amine- Functionalized Mesoporous Domains for Carbon Dioxide Capture,
14 *ChemSusChem* **2016**, *5*, 455-461.
15
16
17 [143] L. Lakiss, F. Ngoye, C. Canaff, S. Laforge, Y. Pouilloux, Z. Qin, M. Tarighi,
18 K. Thomas, V. Valtchev, A. Vicente, L. Pinard, J.-P. Gilson, C. Fernandez,
19 On the remarkable resistance to coke formation of nanometer-sized and
20 hierarchical MFI zeolites during ethanol to hydrocarbons transformation, *J.*
21 *Catal.* **2015**, *328*, 165-172.
22
23
24
25
26
27
28
29
30
31
32
33
34
35
36
37
38
39
40
41
42
43
44
45
46
47
48
49
50
51
52
53
54
55
56
57
58
59
60

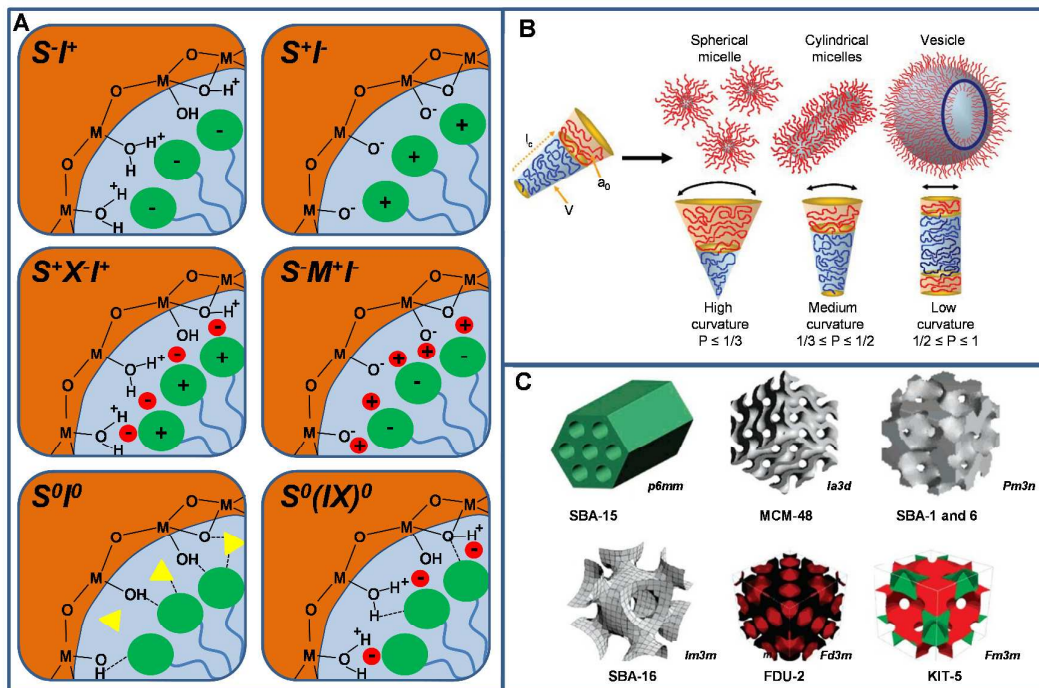


Figure 1. Key concepts of surfactant-templating. Summary of the different chemical interactions leading to mesostructured materials (A). Influence of the mesoporous architecture by the micellar packing parameter (B). Examples of the diversity of mesoporous architectures of amorphous silica (C). Adapted with permission from ref. 9, 11 and 14.

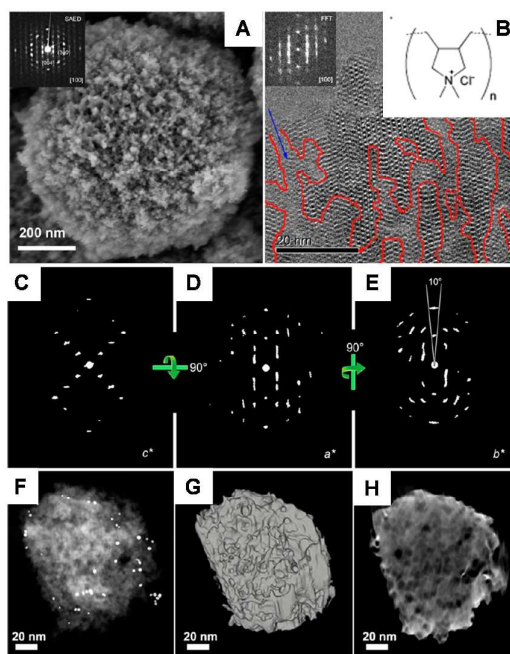


Figure 2. SEM (A) and TEM (B) micrographs of mesoporous *BEA obtained through the employment of PDADMAC. Inset: The chemical structure of PDADMAC. Reconstructed reciprocal lattice of the mesoporous *BEA projected along the c^* (C), a^* (D) and b^* (E) directions. Representative HAADF-STEM image of mesoporous *BEA selected from a tilting series over a range from -75° to $+75^\circ$ at regular intervals of 1° (F). Reconstructed morphology of Beta-MS from HAADF-STEM tomography visualized by surface rendering (G). A slice to the $[001]$ direction extracted from the reconstructed volume (H). Adapted with permission from ref. 36.

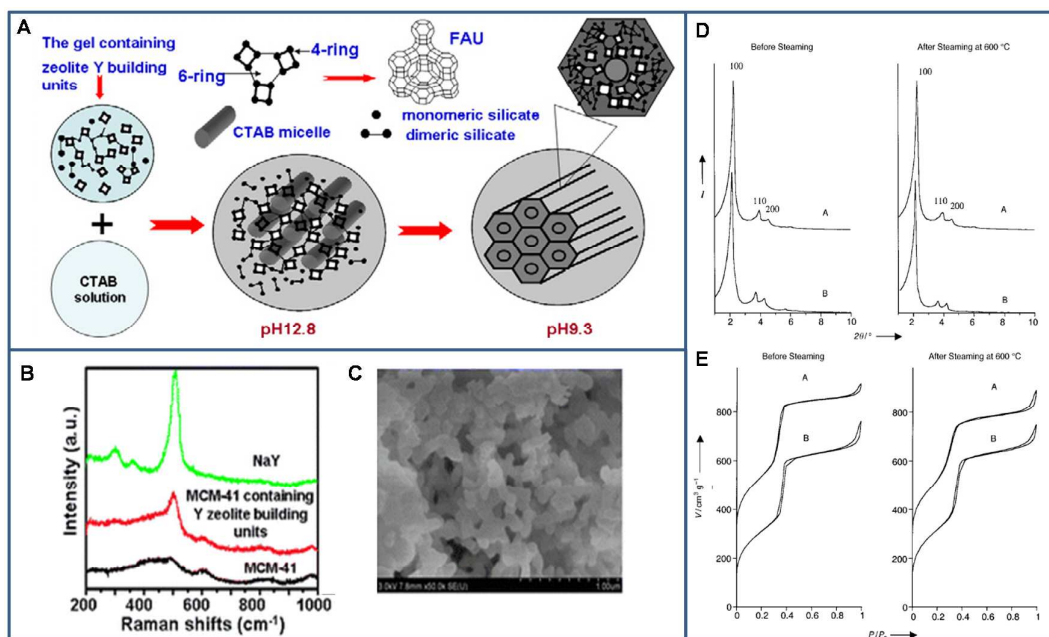


Figure 3. Schematic representation of the formation of Al-MSU-S materials (A). Evidence of the presence of zeolite Y building units by Raman spectroscopy (B). SEM images of Al-MSU-S (C). XRD patterns (D) and N₂ adsorption and desorption isotherms at 77 K (E) before and after steaming (600 °C, 5 h) of mesoporous aluminosilicates Al-MSU-S_{MFI} prepared with ZSM-5 seeds (A) and Al-MSU-S_{BEA} prepared with *BEA seeds (B). Adapted with permission from ref. 43, 46 and 47.

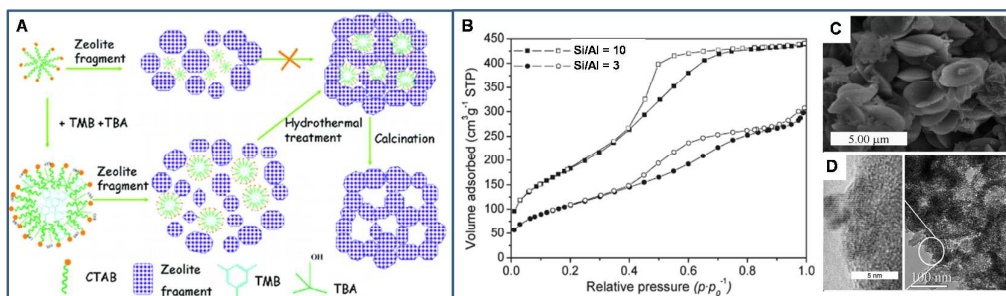


Figure 4. Schematic representation of the mechanism leading to the formation of mesoporous zeolites (A). Nitrogen adsorption and desorption isotherms at 77 K of mesoporous FAU with variation of Si/Al ratio in the synthesis mixture (B). SEM (C) and TEM (D) images of hierarchical FAU. Adapted with permission from ref. 52.

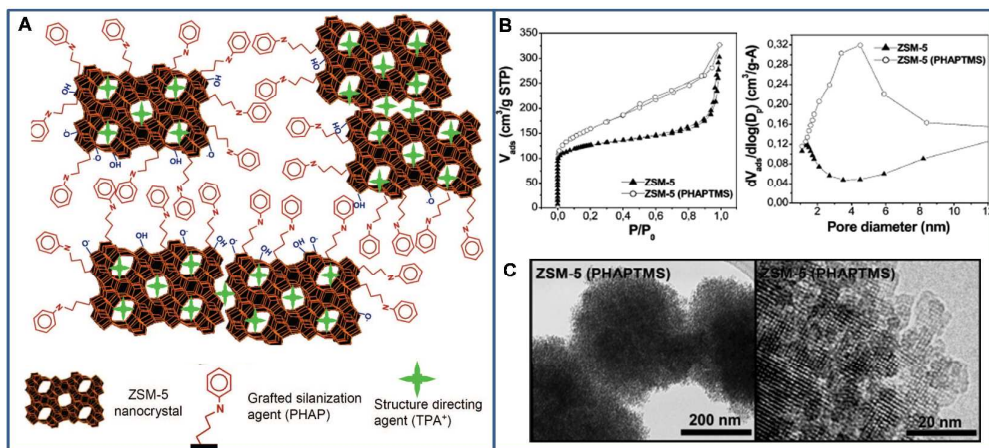


Figure 5. Schematic representation of the ZSM-5 zeolite subunits functionalized with phenylaminopropyl groups (A). Nitrogen adsorption and desorption isotherms at 77 K and BJH pore size distribution of mesoporous ZSM-5 and bulk ZSM-5 (B). TEM micrographs of mesoporous ZSM-5 (C). Adapted with permission from ref. 60 and 61.

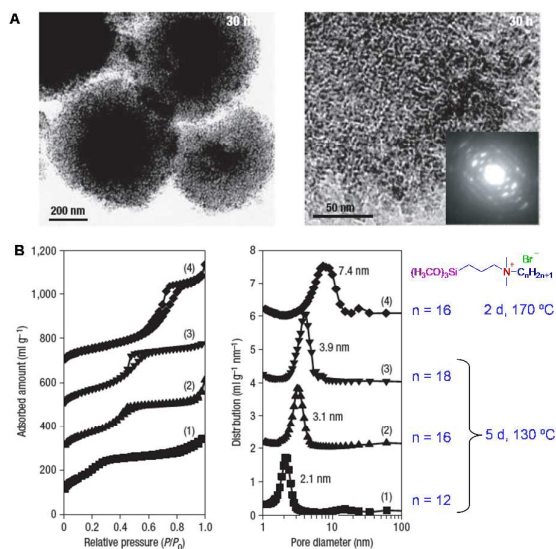


Figure 6. TEM micrographs (A) and nitrogen physisorption isotherms at 77 K and BJH pore size distribution (B) of mesoporous ZSM-5 obtained with surfactants of various chain lengths. Adapted with permission from ref. 64 and 70.

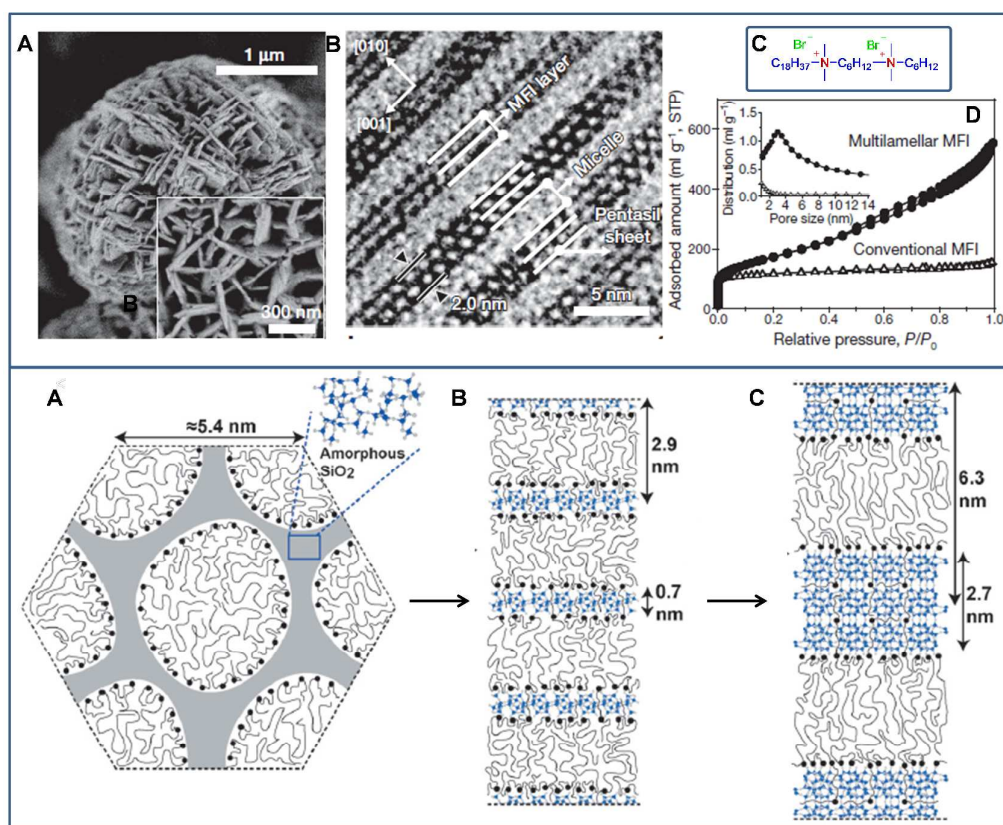


Figure 7. Top: SEM (A) and TEM (B) images of mesoporous MFI nanosheet assemblies. Chemical structure of $C_{22}H_{45}-N(CH_3)_2-C_6H_{12}-N(CH_3)_2-C_6H_{13}Br_2$ (C). Nitrogen adsorption and desorption isotherm at 77 K for bulk MFI and mesoporous MFI nanosheets (D). Bottom: Schematic representation of the development of the atomic and mesoscopic structure during the synthesis of MFI nanosheets. Initially amorphous silica framework (gray) with weak hexagonal mesoporous ordering (A). Intermediate nanolayered silicates (B) and zeolite MFI nanosheets (C). Blue and white spheres: Si and O framework atoms, respectively. Black circles and gray lines: surfactant headgroups and alkyl chain length, respectively. Adapted with permission from ref. 73 and 75.

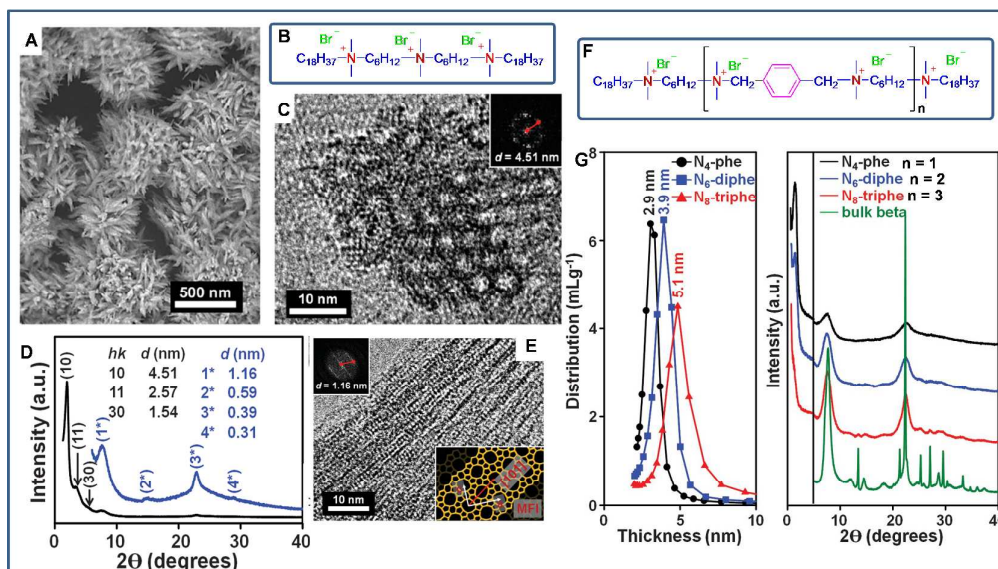


Figure 8. SEM (A) and TEM (C and E) micrographs of hierarchical materials obtained through the use of multicationic surfactants. Insets in C and E are the FFT of these micrographs. Chemical structure of the tricationic surfactant 18-N₃-18 (B). Low and wide angle XRD patterns of achieved materials (D). Structure of the multicationic surfactants featuring aromatic groups (F). Framework thickness and XRD patterns of materials prepared with N₄-phe, N₆-diphe and N₈-triphe. Adapted with permission from ref. 78.

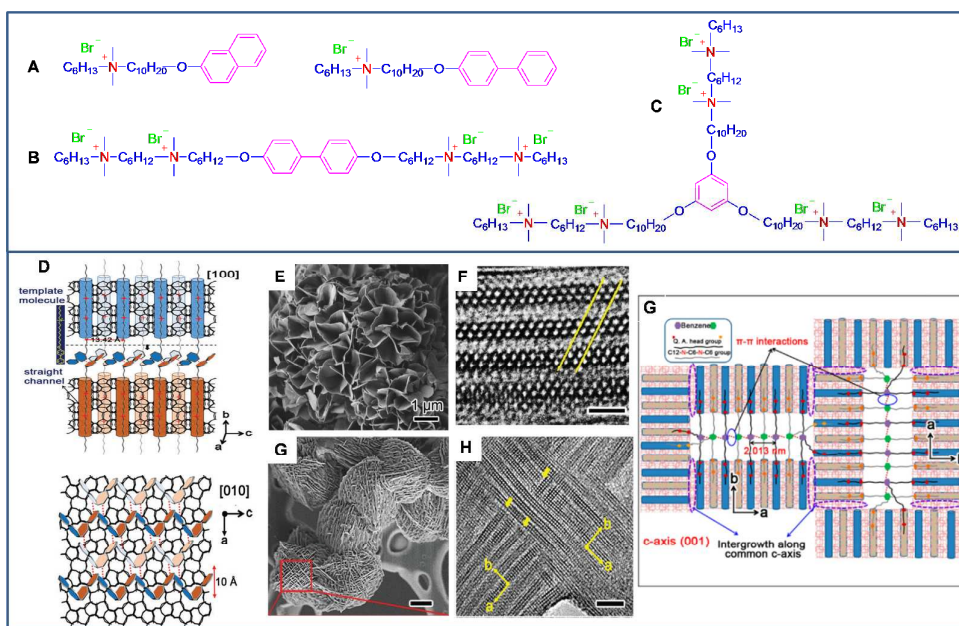


Figure 9. Design concept for the achievement of mesoporous ZSM-5 zeolite. Top: Structures of designed surfactants. Structure of ammonium-based surfactants ended by aromatic groups (A). Bolaform surfactant (B). Triply branched multi cationic surfactants with aromatic center (C). Bottom: Schematic representation of the formation of the nanosheet structure build up through π - π interactions of surfactants depicted in A (D). SEM (E) and TEM (F) micrographs of hierarchical zeolites synthesized with surfactants depicted in A. SEM (G) and TEM (H) micrographs of hierarchical zeolite synthesized with Bolaform surfactant depicted in B. Schematic representation of the formation of three dimensional mesopores zeolites through π - π stacking of surfactant cores depicted in C (G). Adapted with permission from ref. 83 and 84.

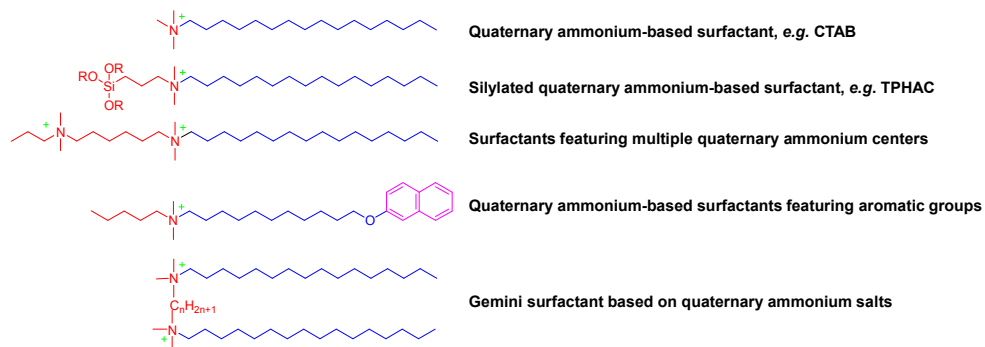


Figure 10. Structures of selected cationic surfactants employed in the development of hierarchical zeolites.

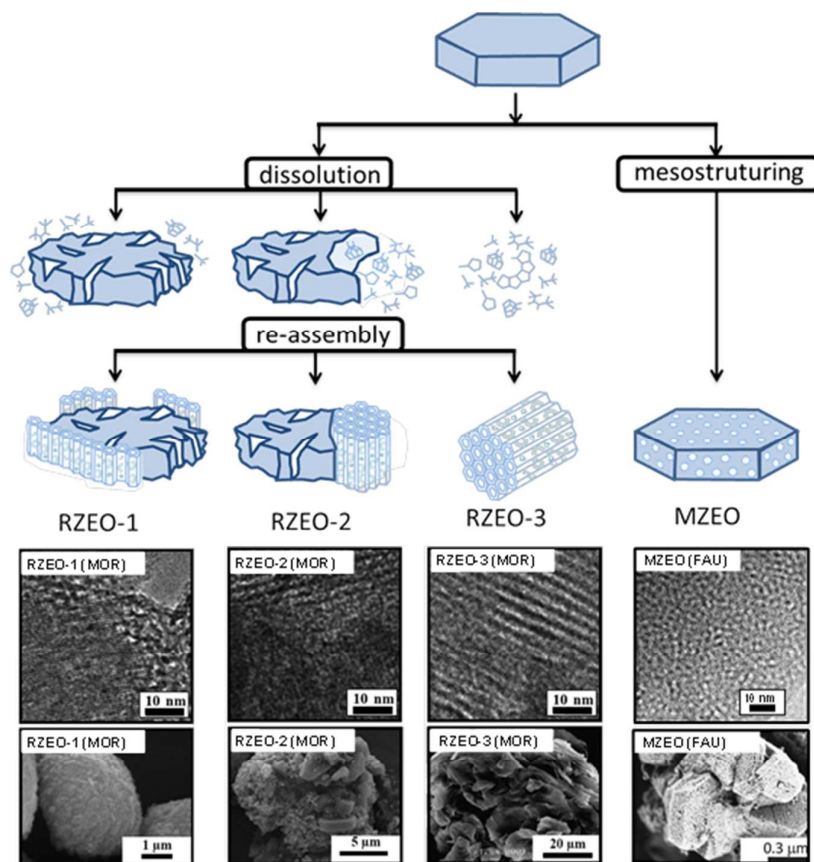


Figure 11. Schematic representation of the post-synthetic approaches using a base and surfactant. On the left side the zeolite recrystallization approach leading to the composite materials RZEO-1, -2 and -3. On the right side the post-synthetic surfactant templating leading to mesoporous zeolites (MZEO). At the bottom TEM and SEM micrographs of the various materials. Adapted with permission from ref. 89 and 100.

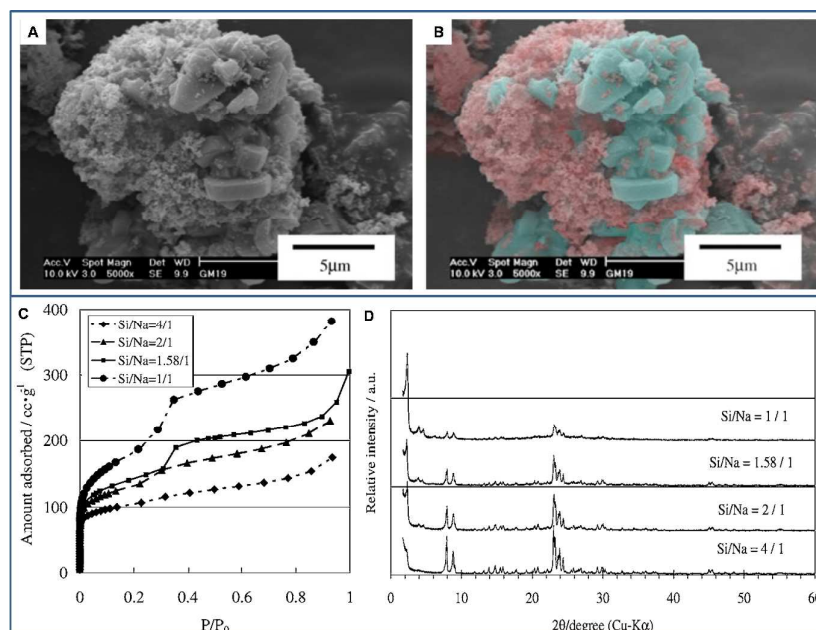


Figure 12. SEM micrograph of MCM-41/ZSM-5 composite material (A). False colored version of the original SEM micrograph, where the amorphous MCM-41 (orange) and crystalline (green) phases are distinguished (B). Nitrogen adsorption and desorption isotherms at 77 K (C) and XRD patterns of composite materials synthesized with different zeolite/NaOH ratios. Adapted with permission from ref. 86.

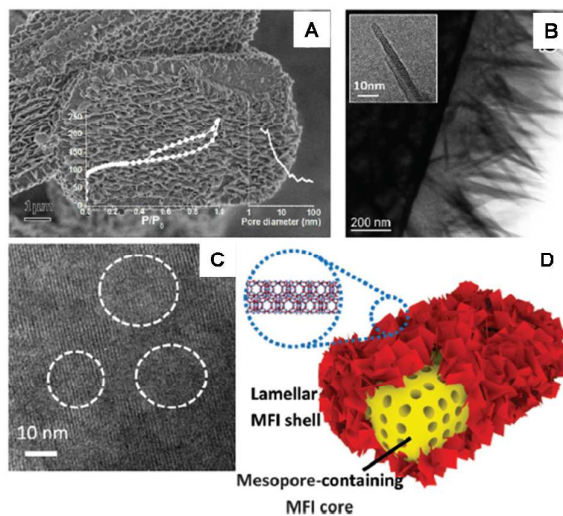


Figure 13. SEM (A), TEM micrographs (B and C) and schematic representation (D) of the composite titanosilicates featuring the core/shell intersection and the irregular intracrystalline mesoporosity. Reprinted with permission from ref. 96.

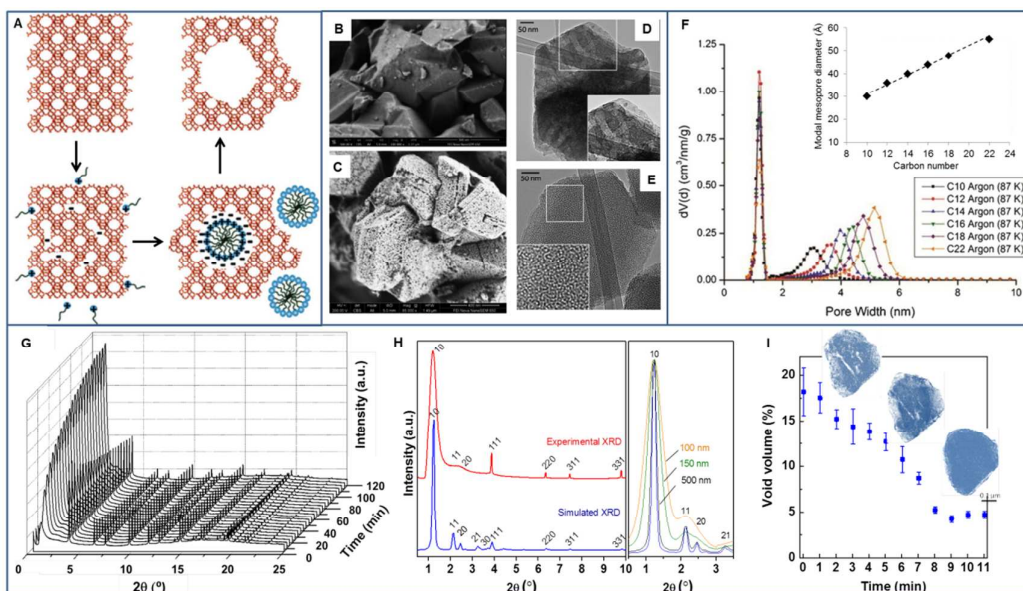


Figure 14. Schematic representation of the proposed mechanism of the post-synthetic zeolite surfactant-templating (A). FESEM micrographs of parent NaY (B) and mesostructured Y (C). TEM micrographs of parent USY (D) and mesostructured USY (E). NLDFT pore size distribution curves calculated from Ar isotherms at 87 K for mesoporous zeolites obtained with trimethylalkylammonium-based surfactants with increasing alkyl chain length (C₁₀ – C₂₂) (F). Inset: linear correlation between mesopore diameter and number of carbon atoms in the surfactant chain. *In situ* time resolved synchrotron XRD study of USY zeolite surfactant-templating (G). Simulated XRD pattern (blue) based on the model shown in (a) and experimental (red) XRD of USY zeolite surfactant-templated. (H). Evolution of the void volume of the steamed porosity in parent zeolite throughout surfactant-templating (I). Adapted with permission from ref. 101 and 118.

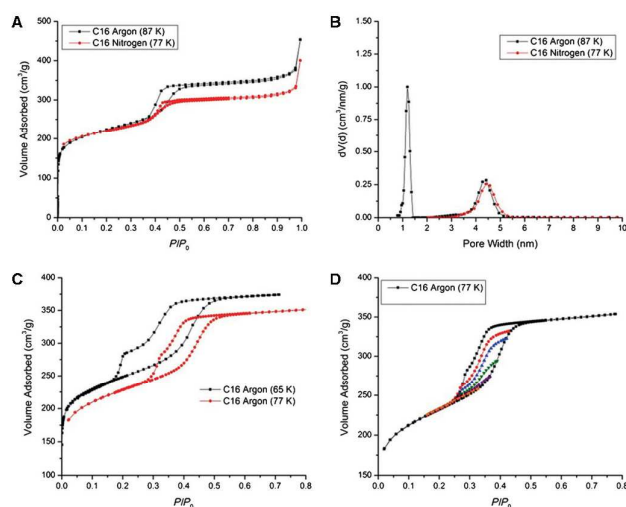


Figure 15. Gas physisorption experiments on surfactant-templated USY with CTAB. Argon (87 K) and nitrogen (77 K) adsorption/desorption isotherms (A). NLDFT pore-size distributions calculated from the argon (87 K) and nitrogen (77 K) isotherms (B). Argon adsorption isotherms at 77 K and 65 K (C). Hysteresis scanning isotherms on the argon (77 K) isotherm (D). Reprinted with permission from ref. 118.

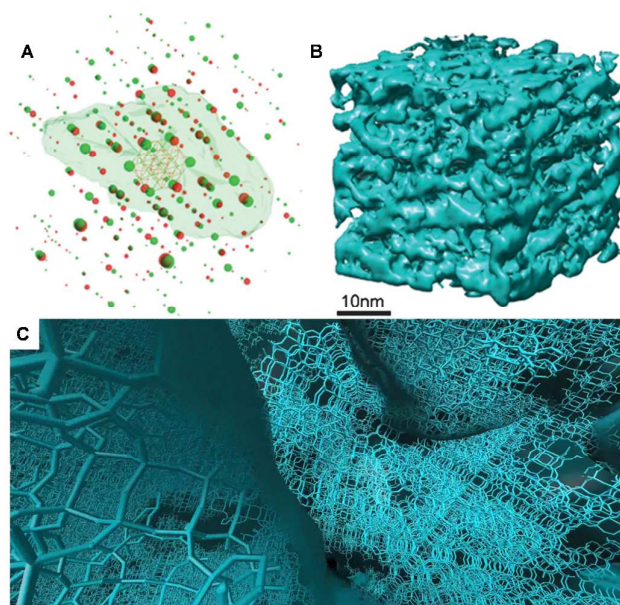


Figure 16. Rotation electron diffraction (RED) and electron tomography (ET) were used to investigate the intracrystalline mesoporous nature of surfactant-templated Y zeolite. Reconstructed 3D reciprocal lattices from the RED data with the reconstructed 3D morphology of the corresponding particle obtained from electron tomography superimposed (A). RED data shows that the particle is highly crystalline zeolite Y with two twin domains (lattices shown in red and green, respectively) sharing a common [111] axis. 3D reconstruction of a portion of a tomogram of mesoporous Y zeolite (B). Frame of the video of the combination of RED and ET (C). Reprinted with permission from ref. 118.

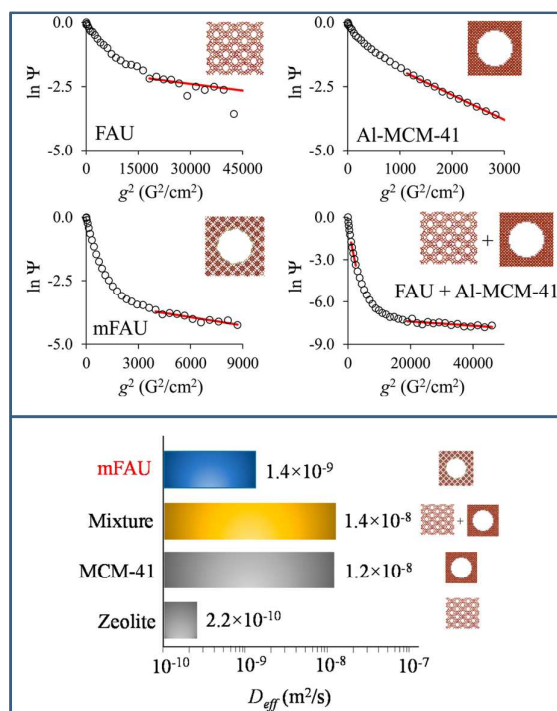


Figure 17. Top: Attenuation Ψ of the spin echo signal as a function of the gradient strength g measured from PFG NMR for hexane adsorbed in FAU, Al-MCM-41, mFAU (*i.e.* surfactant-templated USY zeolite), and a mechanical mixture of FAU + Al-MCM-41. Bottom: Representation of the effective diffusivity D_{eff} as determined from PFG NMR for hexane adsorbed at 298 K in FAU, Al-MCM-41, mFAU, and a mechanical mixture of FAU + Al-MCM-41. Adapted with permission from ref. 119.

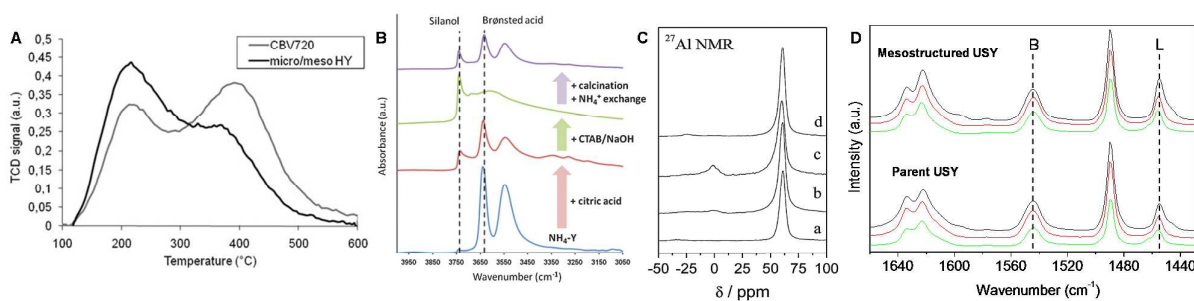


Figure 18. TPD-NH₃ profiles of parent USY (gray) and mesostructured USY (black) (A). FT-IR spectra of Y zeolite sampled along surfactant-templating (B). ²⁷Al MAS NMR of parent Na-Y zeolite (a), after acid pre-treatment (b), after surfactant-templating in the presence of CTAB and NH₄OH solution (c) and after surfactant-templating in the presence of CTAB and NaOH solution (C). FT-IR spectra of pyridine chemisorbed parent USY and mesostructured USY recorded after desorption at 150 °C (black), 250 °C (red) and 350 °C (green) (D). Adapted from ref. 98 and 99.

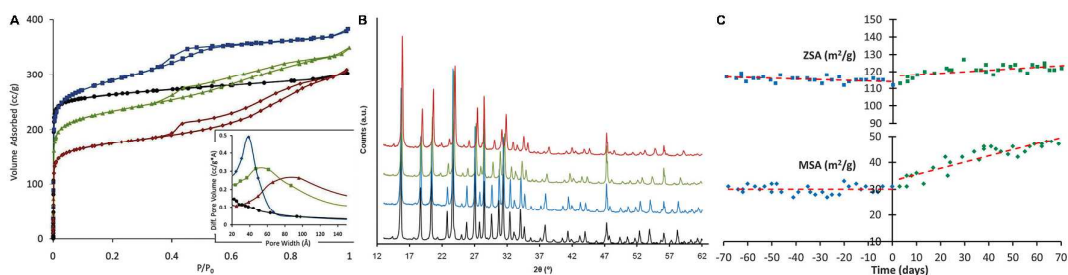


Figure 19. Ar adsorption isotherm at 87 K of NH4-Y (black circle), mesostructured Y (blue square), and mesostructured USY before (green triangle) and after (red diamond) deactivation at 788 1C in 100% steam for 4 hours (A). The corresponding BJH pore size distributions of these samples are shown in the inset. XRD patterns of, from bottom to top, the starting NH4-Y (CBV300), mesostructured Y, the mesostructured USY, and after its deactivation at 788 °C in 100% steam for 4 h (B). The intensities of the last three samples were corrected using a 1.45 empirical factor to account for the radiation absorption by the rare earth oxides (5 wt%) in these materials. Zeolite surface area (ZSA, squares) and mesopore surface area (MSA, diamonds) of the equilibrium catalyst samples gathered from CountryMark Refinery FCC Unit every 2–3 days before (blue) and after (green) the trial started at day 0 (C). Reprinted with permission from ref. 98 and 125.

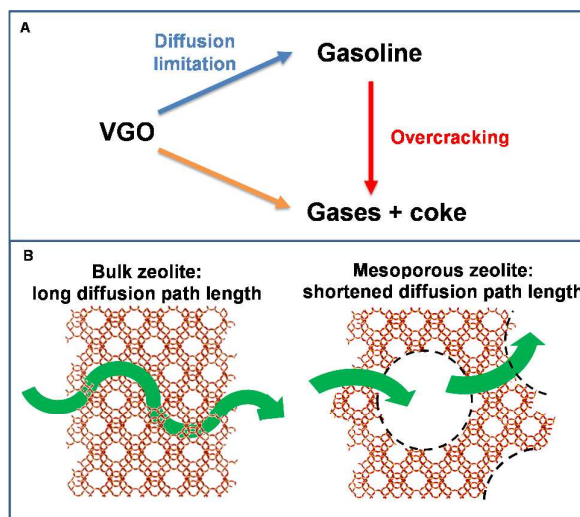


Figure 20. Three-lump model of the catalytic cracking of vacuum gas oil (VGO) (A). In a diffusion limited reaction, overcracking reactions are favored, leading to reduced conversions towards gasoline and LCO and increased selectivity towards undesired light gases and coke. Schematic representation of the diffusion path length in bulk zeolites and in hierarchical zeolites featuring intracrystalline mesoporosity (B).

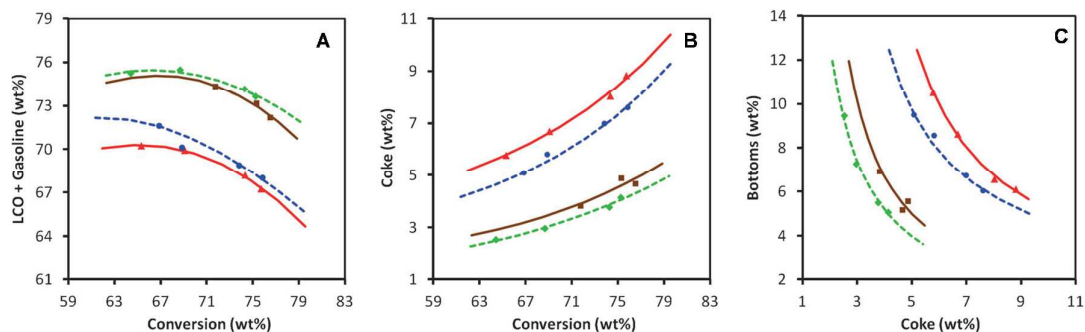
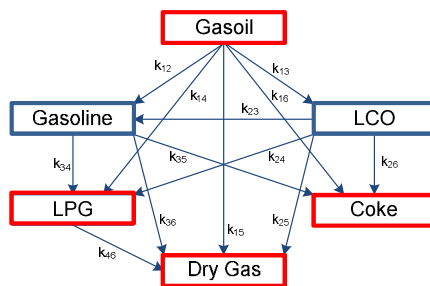



Figure 21. Advanced cracking evaluation (ACE) testing results of two FCC catalysts containing mesostructured USY zeolite to two state-of-the-art catalysts with conventional USY using two different North American refinery feeds. Light VGO feed: FCC catalyst containing mesostructured USY zeolite (green) and Conventional FCC catalyst (brown). Heavy VGO feed: FCC catalyst containing mesostructured USY zeolite (blue) and Conventional FCC catalyst (red). LCO + Gasoline yields vs. Conversion (A). Coke yields vs. Conversion (B). Bottoms yields vs. coke yields (C). Reprinted with permission from ref. 118.



 Increases in presence of intracrystalline mesoporosity


 Decreases in presence of intracrystalline mesoporosity

Figure 22. Six-lump model of the conversion of gasoil. Shortening the diffusion path length in zeolites leads to significant increase in the yield of the desired products (blue) and a decrease in the undesired products (red).

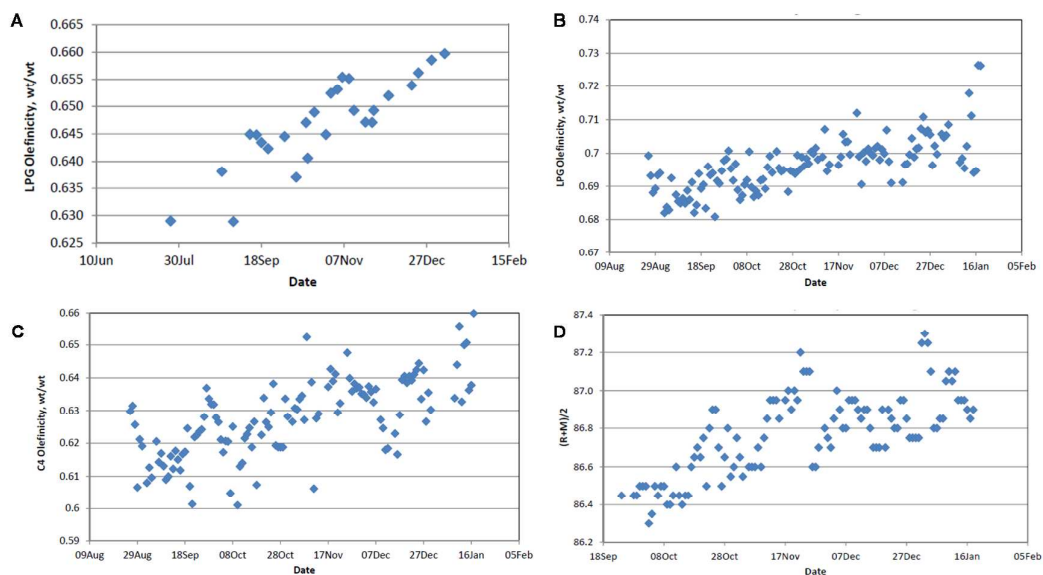


Figure 23. Evolution of LPG olefinicity during a commercial operation obtained in an ACE unit using Ecat from the refinery. Refinery data as the trail evolved on LPG olefinicity (B) C₄ olefinicity (C) and gasoline octane (D). Adapted with permission from ref. 134.

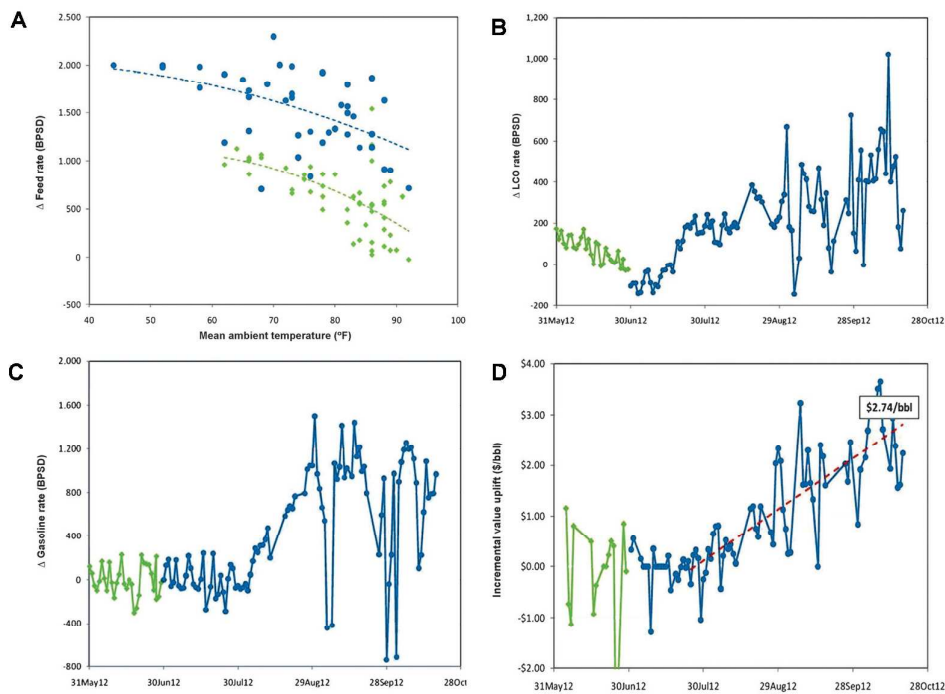


Figure 24. Observed trends during a trial at Alon's Big Spring, Texas refinery: a) Increased feed rate by 700 BPSD (barrel per stream day); b, c) increased production of gasoline and LCO (the big spikes in the plant data were owing to process interruptions and not to the catalyst); d) an incremental value uplift owing to the change-out of the incumbent catalyst for the FCC catalyst containing mesostructured Y zeolite. Adapted with permission from ref. 135.

Graphical Abstract

